Assessing the Quality of Models of the Ambient Solar Wind

MacNeice, P. [1], Jian, L.K. [1], Antiochos, S.K. [1], Arge, C.N. [1], Bussy-Virat, C.D.[3], DeRosa, M.L.[4], Jackson, B.V.[5], Linker, J.A.[6], Mikic, Z.[6], Owens, M.J.[7], Ridley, A.J.[3], Riley, P.[6], Savani, N.[12], Sokolov, I.[3]

[1]Heliophysics Science Division, NASA Goddard Space Flight Center, Greenbelt, Maryland, USA.

[2]institute, University of Maryland, Baltimore County, Maryland, USA.

[3]Department of Climate and Space Sciences and Engineering, University of Michigan, Ann Arbor, Michigan, USA .

[4]Lockheed Martin Solar and Astrophysics Laboratory, Palo Alto, California, USA.

[5]Center for Astrophysics and Space Sciences, University of California San Diego, La Jolla, California, USA.

[6]Predictive Science Inc., San Diego, California, USA.

[7]Department of Meteorology, University of Reading, Earley Gate, Reading, UK.

Key Points:

- Status of models of the ambient solar wind
- Focuses on models relevant to both operational forecasting and scientific space weather research
- Anticipates future developments.

Corresponding author: P. MacNeice, `Peter.J.MacNeice@nasa.gov`

Abstract

In this paper we present an assessment of the status of models of the global Solar Wind in the inner heliosphere. We limit our discussion to the class of models designed to provide solar wind forecasts, excluding those designed for the purpose of testing physical processes in idealized configurations. In addition, we limit our discussion to modeling of the 'ambient' wind in the absence of coronal mass ejections. In this assessment we cover use of the models both in forecast mode and as tools for scientific research. We present a brief history of the development of these models, discussing the range of physical approximations in use. We discuss the limitations of the data inputs available to these models and its impact on their quality. We also discuss current model development trends.

1 Introduction

This paper presents an assessment of the status of models of the solar wind in the inner heliosphere. It is intended to assess progress resulting from the community-wide efforts to create a robust solar wind forecasting capability that can be used in an operational setting. We also identify prospects for future model improvements.

We focus on models which are designed toward a future in forecasting the state of the global inner heliospheric solar wind. We exclude those designed for the purpose of testing physical processes in idealized configurations, although we anticipate how they may impact future developments of the forecast models. In addition, we limit our discussion to modeling of the 'ambient' wind in the absence of coronal mass ejections.

Our assessment is split into 6 sections. The first, section 2, presents a brief history of the development of relevant models from their origin up to the present. Section 3 presents a summary of the current capabilities of the models from both the operational and research user perspective. In section 4 we discuss issues associated with the model inputs and how these are being addressed. Section 5 discusses some physical processes which are still not incorporated into the models, and finally section 6 offers our conclusions.

This paper is designed to illustrate the development history and status of the models, not to be a comprehensive review of the complete literature in the field. In the interest of brevity, the narrative of model history is developed by selecting a few models whose stories serves to illustrate the common development of their model classes.

2 Model History

In this section we briefly review the history of the development of models of the ambient corona and solar wind. In organizing this, we proceed from models with the simplest physical approximations which rely most heavily on empirical tuning, to the most sophisticated. The models we reference are listed in table 1. Those models without an explicit name are listed under the model developer's name(s).

2.1 Empirical Models

Modeling of the solar coronal magnetic field began in earnest in the early 1960's with the advent of computers and the availability of photospheric magnetograms. The earliest models of the inner coronal field were based on current free potential solutions. The potential field source surface (PFSS) approach was developed in the late 60's (*Altschuler and Newkirk* (1969), *Schatten et al.* (1969)) using spherical harmonic expansion (*Gauss* (1839), *Chapman and Bartels* (1940)) of the solution, and extended to include a current sheet by *Schatten* (1971). This work provided the coronal model foundation for the Wang-Sheeley(WS) model. Based on observed inverse correlations between the wind speed and the coronal field expansion factor (*Wang and Sheeley* (1990), *Sheeley and Wang* (1991)), an empirical model of the solar wind speed was developed. With subsequent improvements, including a revised empirical formula which also takes account of the proximity of fieldline footpoints to the nearest coronal hole boundary, the model became the Wang-Sheeley-Arge(WSA) model (*Arge and Pizzo* (2000)). Recently *Riley et al.* (2015) have pointed out that the distance from the coronal hole boundary seems to be more important for accurate models than the expansion factor.

The WSA model uses a spherical source surface which is almost always located at $2.5R_\odot$, where $R_\odot$ is the solar radius. A number of authors (*Schulz et al.* (1978), *Levine et al.* (1982)) have explored the effects of non-spherical source-surface shapes, and *Zhao and Hoeksema* (1994) provided a current sheet source surface (CSSS) model, that includes the effect of a current outside the PFSS domain. Although most modeling efforts use the PFSS model, and it remains the only one in active operational use (*Luhmann et al.* (2002)), there is one notable exception of its use in passive forecasts of field in the HelTomo interplanetary scintillation (IPS) based heliographic tomography model (*Dunn et al.* (2005), *Jackson et al.* (2016)).

Table 1. Models Referenced in this paper.

Model Name	Type	Spatial Domain
PDF	Empirical pattern matching	L1
PROJECTZED	Empirical pattern matching	L1
AnEn	Empirical pattern matching	L1
PFSS	Potential Field	Corona
NLFFF	Force Free Field	Corona
Yeates et al	3D Magnetofriction	Corona
WSA	Potential + semi-empirical kinematic	Corona + Inner Heliosphere
HAF	Potential + semi-empirical kinematic	Corona + Inner Heliosphere
ESWF	Empirical from Coronal Hole EUV	L1
WSA/ENLIL	Potential + 3D MHD	Corona + Inner Heliosphere
HHMS	Potential + 3D MHD	Corona + Inner Heliosphere
Usmanov	Potential + 3D MHD	Corona + Inner Heliosphere
SIP-CESE	Potential + 3D MHD	Corona + Inner Heliosphere
LFM_Helio (now GAMERA)	Potential + 3D MHD	Corona + Inner Heliosphere
CRONOS	Potential + 3D MHD	Corona + Inner Heliosphere
EUHFORIA	Potential + 3D MHD	Corona + Inner Heliosphere
SUSANOO-SW	Potential + 3D MHD	Corona + Inner Heliosphere
MS-FLUKSS	Potential + 3D MHD	Corona + Inner Heliosphere
REPPU	3D MHD	Corona + Inner Heliosphere
Hayashi	3D MHD	Corona + Inner Heliosphere
CORHEL	Model Suite (Potential and MAS 3D MHD)	Corona + Inner Heliosphere
AWSoM_R	Part of SWMF (Potential and 3D MHD)	Corona + Inner Heliosphere
CGEM	Model Suite (3D Magnetofriction + MHD)	Corona + Inner Heliosphere
HelTomo	3D Tomographic	Inner Heliosphere
ADAPT	Flux evolution	Solar surface
SURF	Flux evolution	Solar surface
AFT	Flux evolution	Solar surface
ESFTM	Flux evolution	Solar surface

WSA has become one of the work-horse models of the research and forecasting communities.

Current operational versions of WSA at both National Oceanic and Atmospheric Administration's Space Weather Prediction Center (NOAA/SWPC) and the Community Coordinated Modeling Center (CCMC) use single synoptic photospheric magnetograms for input. The next version, to be released shortly, will also be able to process time evolving series of synoptic maps produced by the Air Force Data Assimilative Photospheric Flux Transport (ADAPT) project (see section 4).

The Hakamada-Akasofu-Fry (HAF) Model (*Fry et al.* (2001)) is similar in general design to the WSA model and as reported by *Norquist and Meeks* (2010), achieves similar performance for both wind speed and IMF polarity predictions.

The Empirical Solar Wind Forecast (ESWF) model (*Reiss et al.* (2016),*ESWF* (2018)), is based on an empirical relation between the areas of coronal holes as observed in EUV and the solar wind speed forecast at L1 4 days after the coronal hole observations. The ESWF operational tool which is currently running at the University of Graz (*ESWF* (2018)) uses hourly updated images from the Atmospheric Imaging Assembly(AIA) on board the Solar Dynamics Observatory(SDO), and an automated coronal hole detection algorithm.

The WSA, HAF and ESWF models apply extensive empirical tuning in order to achieve their forecast quality. In contrast, models such as the Probability Distribution Function (PDF) model (*Bussy-Virat and Ridley* (2014)), PROJECTZED (*Riley et al.* (2017)) and the Analogue Ensemble (AnEn) model (*Owens et al.* (2017)) are purely empirical.

The PDF model forecasts the wind speed at L1 up to five days in advance using probability distributions which have been constructed by analyzing solar wind observations between 1995 and 2011. These probability distribution functions specify the likelihood that a particular wind speed will occur, given the current speed and the current slope of the wind speed curve. The model also takes account of rotational periodicities at quiet times and was updated (*Bussy-Virat and Ridley* (2016)) to improve its ability to identify stream interaction regions (SIRs). The PDF model has recently been installed at the CCMC.

PDF is just one of a range of possible probabilistic forecasting approaches. *Owens et al.* (2017) provide some initial results using an approach borrowed from the atmospheric weather forecasting community, called the analogue ensemble (AnEn), or 'similar day' approach. In this method, and in a similar model called PROJECTZED (*Riley et al.* (2017)), intervals from the past which 'resemble' the most recent time window are used in ensemble fashion to predict what the wind will look like in the immediate future. Based on their initial evaluation, this approach, as configured in their tests, appears to outperform persistence. *Owens et al.* (2017) conclude that 'the AnEn approach is very promising for short or medium lead-time solar wind and geomagnetic forecasting (hours to days) and thus may serve as a complementary approach to the longer lead-time (days to weeks) physics-based magnetohydrodynamic models.' However their exploration of how best to tune this approach is still in its infancy, and improved performance can be anticipated.

2.2 Force Free Models of the Coronal Field

Potential field models of the corona make the simplifying assumption that the corona has no electrical current. This is not true, but does allow for analytic solutions that match the photospheric field measurements and which can be computed quickly, which is why models based on the potential field approximation, such as WSA, have been and remain so popular.

To properly model currents in the corona requires full magnetohydrodynamic (MHD) modeling. Because MHD models are computationally more intensive and the full complement of boundary conditions (which include photospheric density and temperature information) are typically not available, their algorithmic complexity makes them less robust than simpler models.

A popular compromise approach has been to allow for currents in the corona, but to insist that these are always aligned with the local magnetic field. This means that the Lorentz force which the magnetic field exerts on the plasma, given by $\mathbf{J}\times\mathbf{B}$ is zero, which is why this class of models is called 'Force Free'.

To justify this approach it is argued that the magnetic field dominates the plasma in the corona. This is not true in the photosphere or in the heliosphere. *Gary* (2001) presented a one-dimensional model for the magnetic stratification of the solar atmosphere using observations at different heights, and argued that there is a range of heights in the

solar atmosphere, between the chromosphere and about 100 Mm, where the plasma β, the ratio of plasma pressure to magnetic pressure, is $\ll 1$. Within this height range, the magnetic pressure is so much larger than gas pressure that neither gas pressure gradients nor the gravitational force can effectively balance any Lorentz forces which might develop and therefore, if the field is in an equilibrium configuration, it must be approximately force free.

Aly (1989) and *Amari et al.* (1997) introduced many of the constraints to which practical force free models, based on observation should adhere. Since then a number of different algorithms have been applied or developed (see the reviews in *Wiegelmann* (2008), *Wiegelmann and Sakurai* (2012)). A number of papers were published in the early 2000's testing these algorithms on analytically constructed test solutions (*Schrijver et al.* (2006), *Metcalf et al.* (2008), *Schrijver et al.* (2008), *DeRosa et al.* (2009), *DeRosa et al.* (2015)). These codes require vector magnetogram data. However prior to the HINODE and SDO missions very little usable vector magnetogram data existed. *Regnier and Fleck* (2004) and *Wiegelmann et al.* (2005) published the first force free models based on actual observations for limited size fields of view containing a few targeted active regions.

Non-Linear force free models were originally developed to understand the build up of free energy in active regions. More recently these models have been extended from cartesian to spherical geometry, and applied to large field-of-view data and even to the global coronal field (*Tadesse et al.* (2014)).

Yang et al. (1986) pointed out that the time independent non-linear force free field problem can be solved by using a time dependent MHD code in which the plasma velocity has been replaced with a frictional force which is proportional to the Lorentz force. This is called the 'magneto-frictional model'. The standard non-linear force free field solution is achieved if the system is allowed to reach an equilibrium.

Since then, *Mackay and van Ballegooijen* (2006) and *Yeates et al.* (2008) have coupled a global magneto-frictional code to a surface flux transport model (*Yeates et al.* (2007)) to create a time dependent quasi-static evolution of the coronal field. This follows the evolution of the coronal magnetic field through a sequence of nonlinear force-free fields in response to the observed photospheric field evolution and flux emergence. The model

173   aims to follow the long-term continuous build-up of free magnetic energy and electric cur-

174   rents in the corona.

175   To date no force free models are in use for operational forecasting. The NLFFF

176   code (*Wiegelmann* (2007), *Tadesse* (2015)) is installed and in use at the CCMC and is

177   part of the SDO product pipeline.

178   In anticipation of their application to SDO Helioseismic and Magnetic Imager (HMI)

179   photospheric vector magnetogram data, the performance of many of these codes was an-

180   alyzed. *Schrijver et al.* (2006) considered their performance when applied to synthetic

181   data with known solutions and guaranteed force-free conditions at the lower boundary,

182   and found them to be reliable and accurate. Applying these techniques to more realis-

183   tic modeling data (*Metcalf et al.* (2008)) and to real vector magnetograms from Hinode

184   SOT-SP (*DeRosa et al.* (2009)) indicated several issues with the NLFFF paradigm.

185   They concluded that four conditions were likely to improve the chances for success-

186   ful application of NLFFF models. These were,

187   - that they cover large volumes at high resolution to minimize the influence of side

188   boundaries,

189   - that they accommodate measurement uncertainties (in particular in the transverse

190   field component) in the formulation of the lower boundary condition,

191   - that they pre-process the lower-boundary vector field to achieve near force-free

192   field as would be found in the high chromosphere, and

193   - that they assimilate coronal observations to constrain the solutions, such as dis-

194   cussed in *Malanuschenko et al.* (2012) and *Malanuschenko et al.* (2014).

195   Additionally, the use of higher-resolution boundary data are shown to benefit estimates

196   of free energy and magnetic helicity within the NLFFF solutions (*DeRosa et al.* (2015)).

197   As discussed above, some of these code improvements have already been developed and

198   SDO now provides a large dataset of full disk vector magnetogram data.

199   Recently, *Peter et al.* (2015) challenged the use of these codes for the purposes of

200   estimating the magnetic free energy in active regions. They analyzed the order of error

201   in the approximation to be equal to the value of β, and confirmed this by comparing their

202   results with the equivalent solutions from an MHD code. They found the error in total

energy to be of the same order as the estimated total free energy. This suggests that to be useful in supporting models of the ambient solar wind, force free models should be supported by imaging analysis of active region loops, as suggested by *Peter et al.* (2015), and tested by *Chifu et al.* (2017) (see also *Warren et al.* (2018)), or should be extended to include both gas pressure gradients and gravity as in magneto-hydro-static equilibrium models (*Zhu and Wiegelmann* (2018)).

2.3 Tomographic Solar Wind Reconstruction Models

For a general review of the development of tomographic techniques for the reconstruction of the solar wind state we refer to *Jackson et al.* (2011).

The state of the art in this area is the University of California San Diego (UCSD) IPS heliospheric 3-D reconstruction inversion tomography (HelTomo) code. Originally developed by *Jackson et al.* (1998), and modified into a time-dependent code in later versions (*Jackson et al.* (2002)) HelTomo is based on matching observed scintillations of astronomical radio sources that are viewed through the intervening solar wind plasma. Because the solar wind plasma contains both the ambient wind and occasionally CMEs, CMEs are imbedded in the observations and cannot easily be separated from the ambient. HelTomo sets up a trial solar wind state at a 'source surface' or inner boundary, typically set to be 15 solar radii. The wind state at the source surface is then propagated outward, using a simple kinematic approximation, to define a 3-D heliospheric model of density and/or velocity. This reconstruction is then used to compute the scintillations expected from the set of astronomical radio sources. The predicted scintillations are compared with actual observations along each radio source line of sight. Differences between the predicted and observed scintillation patterns are then used, in an iterative process to update the solar wind state at the inner boundary, until a good match is achieved between observation and forecast. This original HelTomo algorithm has since been extended to incorporate in-situ wind speed (*Jackson et al.* (2010)) and density (*Jackson et al.* (2013)) measurements as constraints in the tomographic reconstruction . The UCSD group maintains a web site where they post nowcasts and forecasts of the state of the solar wind (http://ips.ucsd.edu/high_resolution_predictions).

For many years the model has been based on scintillation data from the Institute for Space-Earth Environmental research (ISEE) STELab radio array in Japan. The Hel-

Tomo team are in the process of extending their data sources to include data sets from other observatories around the globe, including from the Ooty array, the Big Scanning Array (BSA) in Russia, the Mexican Radio Array Telescope, the Murchison Widefield Array in Western Australia, and the Low Frequency Array based in the Netherlands. Inclusion of observations from other observatories can provide a potentially much larger data sets that the ISEE IPS system can alone provide, and in addition will benefit from more-continuous coverage of the solar wind condition near the Sun.

They have also been experimenting with use of more sophisticated wind propagation methods, such as the ENLIL MHD code, both as an upgrade to the HelTomo model, and as a method to initialize the MHD models of the solar wind with a more accurate starting state (*Yu et al.* (2015), *Jackson et al.* (2015)). This IPS-driven ENLIL system is run in real-time at both George Mason University and the Korean Space Weather Center). The advantage of this system is that it can show and forecast the propagation of both ambient solar wind structures as well as CMEs without human intervention.

HelTomo was one of the first solar wind models presented to the CCMC at the Goddard Space Flight Center circa the year 2000.

2.4 MHD codes

The first 3D MHD model of the ambient global corona and heliosphere based on photospheric magnetic field data was that of *Usmanov* (1993). This model used a PFSS model to initialize the inner coronal field and set surface boundary conditions. It divided the full simulation into two domains, an outer region of supersonic/super-alfvenic flow from $r^* = 9.8R_\odot$, and an inner region from the surface to r^*, with different algorithms applied to the two regions.

This approach of coupling different codes beyond the sonic and alfvenic points has been followed in almost all MHD solar wind models since then. In some cases, the inner region is modeled using WSA, and the outer region using an MHD algorithm (e.g. ENLIL(*Odstrcil* (2003)), HHMS(*Detman et al.* (2006)), GAMERA (previously known as LFM_Helio, *Merkin et al.* (2011)), CRONOS (*Wiengarten et al.* (2013)), EUHFORIA (*Pomoell and Poedts* (2018)), SUSANOO-SW (*Shiota et al.* (2014)), and MS-FLUKSS (*Kim et al.* (2018)). In other cases MHD codes are used for both regions (e.g. CORHEL,

²⁶⁴ AWSoM_R(*van der Holst et al.* (2014)), SIP-CESE MHD(*Feng et al.* (2012)), *Hayashi*

²⁶⁵ (2012), REPPU (*Nakamizo et al.* (2009), *Den et al.* (2015)).

²⁶⁶   Over the last 20 years these MHD codes have evolved to improve the physical pro-

²⁶⁷ cesses that are included, to improve the underlying algorithms, their user interfaces and

²⁶⁸ the efficiency with which they execute. The development history of the MHD about a

²⁶⁹ Sphere (MAS) code, which is part of the CORHEL model suite, offers a typical illustra-

²⁷⁰ tion of the discipline's progress.

²⁷¹   In 1999, *Mikic et al.* (1999) used a 3D MHD code (MAS) with an adiabatic energy

²⁷² equation and a reduced polytropic index to model the global corona out to $30R_\odot$. They

²⁷³ used a polytropic equation of state for simplicity, with a reduced value of $\gamma = 1.05$, based

²⁷⁴ on Parker's (1963) observation that the coronal temperature does not vary significantly.

²⁷⁵ Not surprisingly, such a simple energy equation fails to reproduce the fast/slow flow speed

²⁷⁶ contrast, (see also *Cohen* (2017)), and the contrast in temperature and density observed

²⁷⁷ between streamers and coronal holes. These flaws were addressed by improving the en-

²⁷⁸ ergy equation in the model to include parallel thermal conduction along the magnetic

²⁷⁹ field lines, radiative losses, and a coronal heating source. This has been called the 'ther-

²⁸⁰ modynamic' model.

²⁸¹   In 2001 *Lionello et al.* (2001) demonstrated a 2D version of the thermodynamic

²⁸² MAS code, and in 2003 *Lionello et al.* (2003) presented initial 3D results from the ther-

²⁸³ modynamic MAS code for the global corona. *Riley et al.* (2001) published a coupled model

²⁸⁴ of the corona and heliosphere that applied the MAS 'polytropic' code separately in the

²⁸⁵ corona and heliosphere, but reprocessed the solution at the outer boundary of the coro-

²⁸⁶ nal component to provide inner boundary flows of the right order for the heliosphere.

²⁸⁷   In 2011 *Riley et al.* (2011) modeled the coupled corona/heliosphere with both poly-

²⁸⁸ tropic and thermodynamic versions, and concluded that the 'empirically adjusted' poly-

²⁸⁹ tropic code still outperformed the physically more complete thermodynamic version. More

²⁹⁰ recently, *Lionello et al.* (2013) introduced turbulent alfven wave heating to the model

²⁹¹ and *Lionello et al.* (2014) validated a time dependent turbulent alfven wave heating model

²⁹² of the solar wind with the thermodynamic code. *Linker et al.* (2016) have since used ADAPT

²⁹³ maps to drive a time dependent MAS solar wind model coupled to the WSA coronal field

²⁹⁴ model. Approaches have been developed to add embedded flux ropes into the coronal

²⁹⁵ field solutions to allow for the influence of large filament structures on the global field

topology (*Titov et al.* (2014),*Titov et al.* (2018)). As the model has been developed, significant work has also been done in developing diagnostic tools to support comparison of model results with observations (e.g. *Downs et al.* (2010), *Winebarger et al.* (2014), *Gibson et al.* (2016)), and to analyze the complex magnetic topologies (*Titov* (2007)).

While the PredSci(PSI) team was developing the CORHEL model suite and its component codes, other models were following similar development tracks and developing comparable capabilities. The University of Michigan group led by Professor Tomas Gombosi developed the Space Weather Modeling Framework (SWMF) (*Toth et al.* (2005)) built around their BAT-S-RUS MHD code (*Powell et al.* (1999), *Gombosi et al.* (2001)). It incorporates a model of the coupled corona and inner heliosphere, supporting a similar range of physical processes (*Roussev et al.* (2003), *Toth et al.* (2005)) as CORHEL, and includes alfven wave heating in the AWSoM_R model version (*van der Holst et al.* (2014), *Meng et al.* (2015)). In addition it can represent multiple species with different gyro-tropic temperatures. *Wiengarten et al.* (2016) have also coupled their CRONOS (*Wiengarten et al.* (2013)) code to equations for the evolution of turbulent alfvenic fluctuations.

In 2004, Arge and Odstrcil began working to couple WSA with Odstrcil's 3D MHD model of the heliosphere which was subsequently named ENLIL. The coupled WSA/ENLIL model has become one of the workhorse models of both research and forecast communities (see *Sheeley* (2017)). As of April 2018, the CCMC has used these models to service more than 7000 user requests for ambient solar wind runs and has executed more that 20,000 near realtime WSA/ENLIL runs to fed its Integrate Space Weather Analysis (ISWA) system. In 2011 WSA/ENLIL was made operational at NOAA SWPC (*Pizzo et al.* (2011)).

Odstrcil et al. (2004) described a similar coupling of the ENLIL heliospheric model with the MAS coronal model. *Merkin et al.* (2016) described a coupling of the LFM_Helio heliospheric model with the MAS coronal model.

3 Assessment of Current Model Capabilities

In this section we present a summary of the capabilities of the current generation of models available for either operational forecasting use, or for use by users through the services of the CCMC. It should be noted that this review relies on validation and qual-

ity assessment studies done in some instances by the model's developer and in others, independently by the community or the CCMC.

We begin in 3.1 by reviewing results on the quality of forecasts at L1 of the empirical models, WSA, PDF, PROJECTZED and AnEn. These models are inexpensive to run and focus on a limited set of wind parameters. It is easy, therefore, to generate formal metric based assessments for these models covering forecasts of specific parameters for long time intervals, resulting in clear quantitative model scores.

For more computationally expensive MHD codes, the validation literature is much less coherent. It consists of multiple studies using different code combinations, focusing on different features of the wind solution, using different methodologies and covering different time periods. We summarize this with a review of the literature in 3.3, and where possible, connect the reported performance levels to the quantitative assessment of the empirical codes.

The MHD codes are capable, when pushed to their limits by their developers, of more sophisticated scientific modeling, than is examined in any of the validation studies. We discuss the most important of these capabilities in subsections 3.4 to 5.1.

3.1 Assessment of Empirical Near Real Time Models

We illustrate the quality of empirical models by concentrating on the WSA , PDF, PROJECTZED and AnEn models. PDF, PROJECTZED and AnEn are purely empirical models which can forecast solar wind properties for which there is an extensive observational record at L1.

The PDF model forecasts wind speed up to five days in advance. It develops probability distributions which are constructed by analyzing solar wind observations between 1995 and 2011. The probability distributions specify the likelihood that a particular wind speed will occur, given the current speed and the current slope of the wind speed curve. The model also takes account of rotational periodicities at quiet times and was updated (*Bussy-Virat and Ridley* (2016)) to improve its ability to identify SIRs.

The PROJECTZED model considers a forecast window Δt. It identifies the observations from the most recent Δt interval, then slides that window backwards in time, 1 hour at a time, comparing each window's observations with the most recent. It uses

357 the OMNI database going back to the early 1970s. It saves the 50 windows that best match

358 the most recent window, and uses the period Δt following each of these, to produce a

359 forecast ensemble for the upcoming window. The mean of this ensemble is the models

360 forecast. PROJECTZED can forecast wind speed, proton number density and temper-

361 ature, and components of the magnetic field.

362 AnEn uses a similar approach but can perform multi-variable pattern matching (for

363 example forecasting wind speed by simultaneously matching both wind speed and pro-

364 ton number density), and allows the user to vary the number of past intervals included

365 in the ensemble. It can also forecast wind speed, proton number density and components

366 of the magnetic field.

367 The essential results, which we detail in 3.1.1 to 3.1.3, are that for the plasma pa-

368 rameters and for the radial and tangential components of the IMF, for forecast windows

369 of 6 hours or less these models work well. For longer forecast windows they continue to

370 outperform both persistence and climatological (the average observed value over time)

371 before eventually approaching the climatological forecasts for windows of approximately

372 100 hours and longer. These quantities are typically determined by the larger scale fea-

373 tures of the wind with temporal coherence of hours to days, and so the pattern match-

374 ing techniques can work effectively.

375 However the processes that establish the component of the IMF out of the plane

376 of the ecliptic, B_N (in RTN coordinates), are generally short scale both spatially and tem-

377 porally. As a result the pattern matching techniques are poorly suited to forecast it. For

378 B_N, while some models do slightly better that the climatological model ($B_N = 0$) for

379 forecast windows of 6 hours or less, they are typically no better than the climatological

380 forecast for longer times.

3.1.1 Wind Speed Forecasts

382 *Owens et al.* (2017) compared the AnEn median model forecast for solar wind speed

383 at L1 to the OMNI hourly dataset and computed the root mean square error (RMSE).

384 For the period from January 1996 through December 2014, for a 24 hour forecast, the

385 AnEn model achieved an RMSE of 48 km.s^{-1}. RMSE is not reported by *Riley et al.* (2017)

386 for PROJECTZED, but its methodology is sufficiently similar to that of AnEn, that we

387 would except a similar result. For the PDF model *Bussy-Virat and Ridley* (2014) report

RMSE for a 24 hour forecast of 83 km.s^{-1} for the year 2008 and 66 km.s^{-1} for the year 2011, illustrating how pattern matching model forecast quality can depend on the time period being studied. For reference, the persistence model achieves an average RMSE of approximately 70 to 80 km.s^{-1} for a 24 hour forecast.

Thus for the pattern matching models for the 24 hour L1 wind speed forecast, over an extended period, the RMSE is expected to be in the range from 50 to 80 km.s^{-1}.

For an older version of the WSA model, *Owens et al.* (2005) report annual RMSE for 24 hour forecast for the years between 1995 and 2002, with model runs made using photospheric synoptic magnetograms from the Mount Wilson Observatory. The yearly averages ranged from 76 to 109 km.s^{-1} with an average of 93 km.s^{-1}.

For a short interval from 2011 to 2014, *Reiss et al.* (2016) found that for 4 day forecasting the ESWF gave an RMSE of 108 km.s^{-1} while for that period WSA gave 99 km.s^{-1}.

As the forecast window increases, the performance of the pattern matching models deteriorates but always beats the persistence model. In contrast the WSA model performance stays relatively constant, apparently independent of the length of the forecast window. For forecast windows less than 3 days it is outperformed by the pattern matching models, but for longer windows it matches their performance. For windows longer that 3 days all models approach the performance of the 'climatological' forecast which assumes that the wind is always at the average observed wind speed.

We can also judge these models based on their ability to forecast events such as High Speed Events (HSEs) where the wind quickly transitions from slow to fast speed, and crossings of the heliospheric current sheet (HCS). *Bussy-Virat and Ridley* (2016) studied PDF and WSA forecasts for HSEs between 1995 and 2012. They report that if a HSE occurred in the next 24 hours, the PDF model made a successful forecast (a 'hit') 20% of the time and 'missed' 80% of the time. 33% of its forecasted HSEs were false positives. When forecasting no HSE in the next 24 hours the model was correct approximately 90% of the time. When they compared the PDF results with those of WSA, they found similar rates of hits and misses, and for forecasting that no event would occur, but found that WSA had 3 times more false positives. These results clearly depend to some extent on how you define a HSE and what criteria you use to determine hits and misses, but

418   the WSA results that they report are generally consistent with those of *MacNeice* (2009b)

419   and *Owens et al.* (2005).

420   The different time windows and methodologies used to analyze both the RMSE and

421   events forecasts highlights a need for a consistent validation.

3.1.2   Wind Density Forecasts

423   For forecast windows of 2 hours or less, persistence outperforms the AnEn model

424   wind density forecasts, but for all longer forecast time windows AnEn always beat both

425   persistence and climatological. For a forecast window of 24 hours it achieved an RMSE

426   of 2.5 cm^{-3}. For forecasts of 80 hours and beyond the wind density RMSE asymptotes

427   to a value of 3 cm^{-3} compared to the climatological value of 3.5 cm^{-3}.

3.1.3   Magnetic Field Forecasts

429   Forecasting the interplanetary magnetic field (IMF) and particularly its north-south

430   component is of most interest for interplanetary coronal mass ejections (ICMEs) (see *Sa-*

431   *vani et al.* (2018)). Occassionally however, and particularly during the declining and so-

432   lar cycle minimum phases, co-rotating interaction regions (CIRs) can introduce a suf-

433   ficiently strong southward component in the ambient wind to produce geo-effective dis-

434   turbances (*Echer et al.* (2017)).

435   Both AnEn and PROJECTZED also forecast the components of the IMF at L1.

436   AnEn reports results for the components of **B** in RTN coordinates, with B_N rep-

437   resenting the out of ecliptic plane component and B_T the component in the plane of the

438   ecliptic. For B_T the relative performance of AnEn compared to both persistence and re-

439   currence is qualitatively similar to that for wind speed, in that the model outperforms

440   both for all forecast windows, but approaches the climatological forecast for time win-

441   dows of order 100 hours. Persistence beats climatological for forecast windows of less that

442   15 hours, but for longer windows climatological significantly outperforms persistence.

443   For B_N however, which is generally of more significance to forecasters, the pattern

444   is markedly different. Persistence outperforms climatological only for forecast windows

445   of less than 2 hours. This is due to the known short autocorrelation time in the observed

446   B_N time series (e.g. *Lockwood et al.* (2016)), and illustrates the challenge associated with

predicting B_N. AnEn outperforms climatological for forecasts of 10 hours or less, beyond which it tracks but is slightly worse than climatological.

Riley et al. (2017) report similar qualitative conclusions for the performance of PRO-JECTZED in forecasting the components of the IMF, although, as already noted, they do not report RMSE scores over an extended period of time.

3.2 Comparing Near Realtime Tomography to Empirical Models

There is a very limited set of published results which we can use to compare the HelTomo model with the empirical models. *Jian et al.* (2015) included HelTomo in a list of CCMC hosted models validated for the Carrington Rotations 2056 to 2062, from May to November 2007. They found a wind speed RMSE for HelTomo of 63 km.s^{-1} for the time interval, easily beating 24 hour persistence which returned a RMSE of 83 km.s^{-1}. This suggests that HelTomo ranks between the empirical models and WSA when measured against RMSE forecast. However there is too little published validation data to claim this as a robust relative ranking.

3.3 Literature Review of MHD Model Validation Studies

Validation studies of the MHD models have been done by the model developers and by users of those models which are hosted at the CCMC. These studies have explored a range of metrics examining various locations and structures in the solution. A review of this literature supports the following conclusions, based on the model use of static synoptic magnetograms.

In the corona, comparing the MHD solution with pure PFSS models (e.g. *Wiegelmann et al.* (2017)),

- the MHD code coronal solutions typically reproduce the same large scale structure (i.e. patterns of open and closed flux) as the potential models and the same general location and shape for the neutral line at the base of the HCS streamer base.
- the MHD codes produce more realistic cusp like topologies at the tip of the HCS streamer where the PFSS models produce more rounded structure.

- field lines in the PFSS model are typically shorter than those in their MHD equivalents.

- PFSS models (using the typical source surface radius value of 2.5 solar radii) appear to underestimate the amount of open flux in the heliosphere.

In the heliosphere, validation work has focussed on operational style metrics (typically at L1, but occasionally for very limited time windows at Mars, Mercury, Venus and at the location of spacecraft including Ulysses and STEREO A and B), and on the location and arrival times of SIRs and current sheet crossings at L1.

With few exceptions, such as *Gressl et al.* (2014), the validation studies of MHD solutions for the ambient wind in the heliosphere have used codes driven at their inner boundary by WSA (or an equivalent model) whose outer boundary was extended beyond the alfvenic and sonic points. As a result, the overall structure of the solution has been imprinted by the MHD codes inner boundary condition. Therefore, different heliospheric MHD codes return the same general solution assuming they use the same magnetogram source to feed the WSA component. The heliospheric MHD codes do allow features in the solar wind imposed on their inner boundary to steepen and sharpen, and can represent the development of shear driven fluctuations. The WSA model, with its kinematic propagation approximation cannot do this. However, in all validation work to date, the WSA model has used angular resolution of 1 degree or coarser. At these resolutions the fluctuations at the inner boundary of the MHD code do not sharpen to sufficiently small scales in transit to L1, that we would expect the MHD model RMSE to differ much from that of WSA. The WSA performance, for which there is a more extensive and coherent set of validation studies, therefore serves as a useful guide to, and comparative baseline for, the MHD model performance.

MacNeice (2009b) analyzed the WSA model's performance in reproducing SIR arrival and IMF sector boundary crossings for the period from 1976 to 2008, and found WSA (with current sheet outer boundary located at 5 solar radii) to be worse than persistence for 1 day forecasts but better than persistence for longer forecast windows regardless of magnetogram source. They found that the model reported fewer high speed events (HSE - proxy for SIR arrival) than were observed, with a HSE hit rate of 40% and a false positive rate of 39%. They found the IMF polarity was correctly reproduced approximately 80% of the time, a polarity reversal hit rate of about 60% and a false pos-

507   itive rate of 11%. They found that the WSA performance was slightly degraded when

508   the outer boundary of the current sheet component was located at 21.5 solar radii as is

509   typical when supporting MHD model application in the heliosphere. These results sup-

510   port the conclusion that the WSA model is better at reproducing the magnetic topol-

511   ogy than the details of the wind speed. This result were consistent with similar stud-

512   ies performed by *Owens et al.* (2005) and *Owens et al.* (2008).

513   Given that the WSA model has been empirically tuned to best fit the observed wind

514   solutions at L1, we anticipate that the MHD model of the heliosphere can at best, match

515   the performance of the WSA model. This is indeed what we find. Overall, the MHD mod-

516   els achieve similar performance to the WSA models. They do of course provide much

517   more complete solutions including parameters which WSA does not reproduce.

518   *Gressl et al.* (2014) reported similar SIR arrival time errors for MHD model runs

519   during the year 2007 close to solar cycle minimum. *Norquist* (2013) reported similar re-

520   sults for the WSA/ENLIL model for the years 2007 through 2011, as did *Lee et al.* (2009)

521   for the declining phase of solar cycle 23 and *Jian et al.* (2011) for time windows in both

522   2007 and the declining phase of cycle 23, with greater solar activity. These studies con-

523   sistently report the following conclusions:

524   At L1,

525   • All solar wind models produce the best simulation results for the solar wind speed

526   parameter, with proton temperature poorly reproduced (often off by an order of

527   magnitude).

528   • The interplanetary sector structure (as coded in the radial magnetic-field strength)

529   is well reproduced, but medium scale features, particularly in the neighborhood

530   of the HCS are not so well reproduced.

531   • For all models, the distributions of modeled solar wind parameters significantly

532   differ from the measured distribution.

533   • Model runs from WSA/ENLIL tested with different synoptic magnetic maps show

534   significant differences in predicted arrival time and amplitudes of solar wind struc-

535   tures (e.g. *Riley et al.* (2012)). However, there is no clear trend as to which syn-

536   optic map gives the best simulation results.

- The solutions are sensitive to how polar fields are reconstructed in the synoptic magnetograms

- All models give too small total magnetic-field strengths (typically by a factor of order 2 (*Lepri et al.* (2008),*Stevens et al.* (2012),*Linker et al.* (2017)).

Are these general trends repeated in the few studies based on data recorded at locations other than L1? *Shiota et al.* (2014) compared the solution from SUSANOO-SW for an interval between 2007 and 2009 with observations at L1, along with data recorded by MEX/ASPERA3 at Mars and VEX/ASPERA4 plasma measurements at Venus. Their results suggest that the model performance at the locations of Mars and Venus is comparable to that which the model records at L1.

Jian et al. (2016) used data from Ulysses from 2007 when its orbit took it from an extreme southern latitude to extreme northern latitude. Their RMSE analyses of wind speed indicate that the models outperformed 2 day persistence, with overall performance consistent with studies focussed at L1.

The assessment studies we have cited find no significant systematic difference in solution quality between quiet and active times. It is important to recognize that CMEs can modify the ambient wind in their wake, and so care must be taken in analyzing the quality of ambient wind solutions during solar maximum. Three points should be remembered. First, well constructed assessment studies allow for this by excluding those times. Second, WSA and MHD models using WSA to set their coronal solution, are dependent on the WSA tuning which has evolved over the years but which generally attempts to achieve the best fit over both solar maximum and minimum. Third, the WSA model has been tuned on data over less than 4 full solar cycles and so the current preferred tuning may not work as well for future cycles.

3.4 Eclipse Forecasts and Energization of the Corona

Predictions provide a rigorous test of the capabilities of models. Over the last two decades the group at PSI has taken advantage of total solar eclipses to test their models by predicting the shape of the white-light corona several weeks in advance. Such predictions can be compared with photographs of the corona subsequently taken during the eclipse (*Mikic et al.* (2007),*Rusin et al.* (2010)) as illustrated in Figure 1. Starting with a post-eclipse simulation of the corona after the 3 November 1994 eclipse, twelve pre-

July11, 2010 Total Solar Eclipse

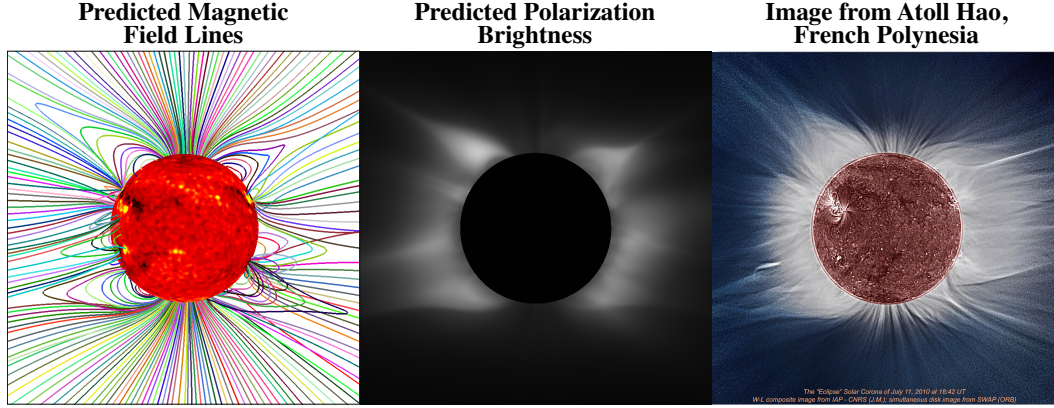| Predicted Magnetic Field Lines	Predicted Polarization Brightness	Image from Atoll Hao, French Polynesia

Figure 1. A comparison between a prediction of the corona, based on the MAS thermodynamic model, for the total solar eclipse of 11 July 2010 (left and center images), and an image of the eclipse (right) taken in French Polynesia (courtesy of Jean Mouette and Serge Koutchmy, Institut DAstrophysique de Paris, France). The images are oriented with solar North vertical.

dictions have been performed, culminating with the recent eclipse on 21 August 2017 (Figure 2). In addition, the corona of the 20 March 2015 eclipse was studied after the fact. A recent investigation compares several models of the corona during this latest eclipse (*Yeates et al.* (2018)).

This collection of PSI predictions is available at http://www.predsci.com/corona, and provides a useful way to track the change in complexity of the solar corona as the Sun evolves between solar minimum and maximum. It also provides an instructive (if somewhat anecdotal) measure of the progress coronal models have made over the last two decades. As discussed in 2.4, starting with a polytropic MHD model of the 24 October 1995 eclipse, the PSI group eventually improved the description of the flow of energy in the corona by implementing a thermodynamic model with empirical coronal heating, including a transition region, radiative losses, and thermal conduction along the magnetic field lines (*Lionello et al.* (2001),*Lionello et al.* (2009)). The latest prediction of the 21 August 2017 eclipse used a wave-turbulence-driven (WTD) heating model (*Verdini et al.* (2010),*Lionello et al.* (2014b),*Lionello et al.* (2014c),*Downs et al.* (2016)) in which the solar wind was accelerated and heated by Alfven waves launched in the chromosphere (see 3.6).

585   The comparison of their results illustrates the extent to which these codes have evolved

586   over the last twenty years and shows the level of physical complexity which they can ac-

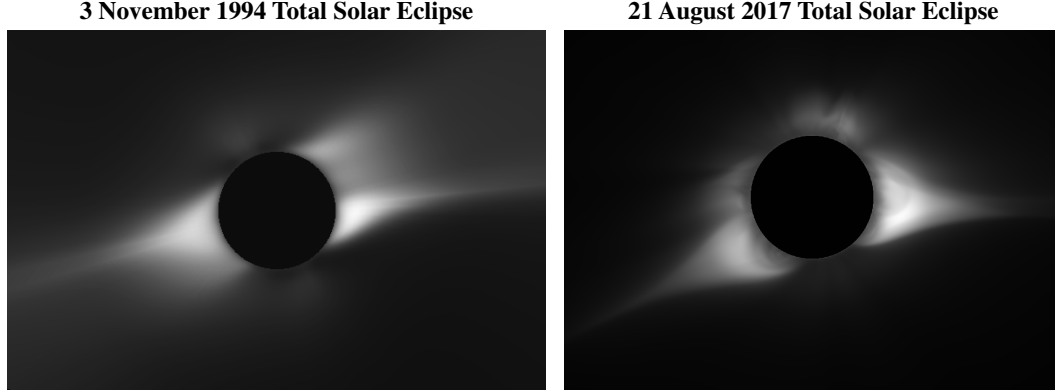587   commodate when pushed to their limits.

3 November 1994 Total Solar Eclipse   **21 August 2017 Total Solar Eclipse**

Figure 2.   Synthesized polarized brightness for the eclipses of 3 November 1994 and 21 August 2017 from the MAS model with thermodynamic energy equation and alfven wave heating.

588   The accuracy of the models has improved over time, as the underlying physical for-

589   mulation was improved, and as computer power increased. The advent of massively par-

590   allel computers significantly improved the spatial resolution of the calculations. These

591   improvements were driven, in large part, as a direct result of comparisons with eclipses.

592   In addition to the white-light comparisons, the wealth of observations from SOHO/EIT

593   and SDO/AIA in EUV wavelengths, and from Hinode/XRT in X-ray wavelengths, made

594   it possible to improve the heating models, through comparisons of synthesized emission

595   with observed emission.

596   For the latest 21 August 2017 prediction, the magnetic field was energized along

597   filament channels, via emergence of transverse magnetic field, followed by flux cancel-

598   lation to create flux ropes. This introduces magnetic shear along the polarity inversion

599   lines (PILs) that are typically the locations at which filaments (prominences) form (*Yeates*

600   *et al.* (2018),*Mikic et al.* (2018)). It produces an 'inflated' appearance of streamers and

601   pseudo-streamers in the lower corona that is typically inferred from eclipse images. The

602   chirality of these flux ropes was determined by running a separate magneto-frictional model

603   (*Yeates* (2014)) for the seven months preceding the eclipse, fed by a surface flux trans-

604   port model (*Upton and Hathaway* (2014)) that assimilated HMI magnetic field data. The

605   locations of the flux ropes were determined by identifying filament channels in images

and movies of SDO/AIA EUV emission. This process increased the free magnetic energy in the corona and led to a more realistic model of the magnetic field in the low corona (*Mikic et al.* (2018)).

The energization of the corona has also been modeled by inserting flux ropes in selected active regions. This was done primarily for the purpose of initiating CMEs, but is relevant for modeling the ambient corona during pre-eruption. PSI have used a modified Titov-Démoulin (TDm) model (*Titov et al.* (2014),*Titov et al.* (2018)) , The group at the University of Michigan have a similar feature, called EEGGL, for CME modeling (e.g. *Jin et al.* (2017)), but because they embed an unstable Gibson-Low flux tube this cannot be used in its current form for ambient coronal modeling.

3.5 Advances in Understanding How to drive Models Directly from Data

The promise of the high cadence and high resolution vector magnetogram data from SDO/HMI led to the hope that these models could be driven directly by the observed temporal evolution of the photospheric field. Significant work has been done to understand how this might be done.

There are two main challenges in preparing the data to drive the MHD coronal field models. First, the data is incomplete for the purpose, and second, there are measurement errors in the data which must be managed so they do not cause the MHD algorithms to fail. It is also the case that the inversion schemes used to produce the vector magnetogram data contain assumptions about the solar atmosphere that affect the resulting vector fields in subtle ways.

In principle, if we can derive the flow and magnetic field vectors on the surface, the time evolving electric field can be computed at the model's lower boundary and this can be used to drive the MHD codes. In practice, because the data does not include vertical gradients of the field and flow vectors, it cannot completely define the field. *Fisher et al.* (2010), *Fisher et al.* (2012) and *Kazachenko et al.* (2014), have developed one method to address this issue. With the inclusion of additional data, such as that from Doppler line of sight velocity measurements taken with HMI, and horizontal flows determined from local correlation tracking (eg *Welsch et al.* (2007)), or other feature tracking approaches like DAVE4VM(*Schuck* (2008)), they have demonstrated that they can return an accurate solution in a test case for which the true electric field is known. This approach is

applied in their Coronal Global Evolutionary Model(CGEM) model suite (*Fisher et al.* (2015)) which will be delivered to the CCMC shortly.

Whatever approach is used to define the surface information, it must then be incorporated into the field model in a manner which is consistent with the algorithm's design, its discretization approach, and its constraint equations. Obviously, codes which use non-spherical coordinates require additional spatial interpolation. To support this processing, *MacNeice and Allred* (2018) developed the MAGIC tools suite which is available for user download from the CCMC website.

It should be recognized that any observational data set inevitably includes measurement errors. Typically the error bars associated with horizontal components of the magnetic field are larger than those associated with the line of sight components. As a result, the observed surface fields are inconsistent with known physical constraints such as the solenoidal condition. The data must be modified to accommodate this before it can be safely applied within the models. It is not yet clear how best to achieve this. In addition there is a known orbital phase signature in the HMI data which has yet to be fully understood (*Schuck et al.* (2016a),*Schuck et al.* (2016b)). The correlation tracking programs require data with a cadence of 12 minutes or less for stable reconstruction, given the HMI pixel sizes (*Leake et al.* (2017)). Their results are therefore impacted by this problem, and until it is corrected, results of models driven directly by this data must be treated with caution.

To date, some attempts have been made with MHD and magneto-frictional codes driven by HMI data to model the evolution of active regions (e.g. *Jiang et al.* (2016), *Hayashi et al.* (2018), *Yardley et al.* (2018)), but have not yet been applied to the global field.

3.6 Physically Motivated Heating, Turbulence and Turbulent Energy

During their early development, almost all multi-dimensional models of the solar wind relied on simple volumetric heating formulae, not connected directly to any specific physical process. Typically they also ignored the energy contained in sub-grid scale turbulence. Over the last half decade global MHD model developers have begun to include the influence of this sub-grid scale turbulence, and coronal and solar wind heating and acceleration sources based on specific physical processes. One example is heat-

668 ing and acceleration due to the dissipation of counter streaming alfven wave fluctuations

669 (e.g. *Chandran et al.* (2011)). The CORHEL (*Downs et al.* (2016)), AWSoM_R (*van der*

670 *Holst et al.* (2014)), CRONOS (*Wiengarten et al.* (2016)) and *Usmanov et al.* (2014) and

671 *Usmanov et al.* (2018) models have all supplemented the basic MHD equations with a

672 set of additional equations describing the energy content, transport and dissipation of

673 the alfven wave fluctuations. These codes have subtle differences. These include how their

674 additional equations are derived, how they relate the energy in the sub-grid scale tur-

675 bulence to shear in the shortest scale fluctuations of their mean flow solution, their es-

676 timates of the energy dissipation rates feeding turbulent energy back into the plasmas

677 internal energy, and the way the alfven wave energy fluxes are set at the inner bound-

678 ary of the models. These modified codes do compare successfully with the general char-

679 acter of the observed corona and solar wind (*Meng et al.* (2015),*Oran et al.* (2017),*Downs*

680 *et al.* (2016),*Usmanov et al.* (2018)).

681 While these developments represent a significant step toward a more complete self

682 consistent physical model, they are based on a description of the turbulence which is greatly

683 simplified. In particular they make numerous assumptions about the form of the turbu-

684 lence spectrum in the inertial range, and impose phenomenological dissipation rates to

685 specify the eventual transfer of energy from the turbulence to the plasmas internal en-

686 ergy. We anticipate that over the next decade, in-situ observations made by the Parker

687 Solar Probe and the Magnetospheric Multiscale Mission will test these turbulence treat-

688 ments and their underlying assumptions.

3.7 Advances in Multi-Fluid Algorithms

690 Heating by dissipation of counter-streaming alfven waves does not heat the elec-

691 trons and ions equally. In addition, observations indicate that the ion distributions have

692 different parallel and perpendicular temperatures. To accommodate both effects, the AW-

693 SoM (*Oran et al.* (2013)) and *Usmanov et al.* (2014) models were developed with sep-

694 arate electron and proton temperatures. *Oran et al.* (2013) found that this gave a hot-

695 ter and faster wind than in the equivalent single temperature model heated by the same

696 Poynting flux injected at the model base. This is principally because electron thermal

697 conduction is more effective than proton thermal conduction. The finite thermal cou-

698 pling between electrons and protons in the two temperature model slows the overall rate

of cooling of the corona by conduction to the radiative sinks of the low corona and transition region.

AWSoM was extended by *van der Holst et al.* (2014) to allow also for distinct parallel proton and perpendicular proton temperatures, and its influence on the solar wind in the inner heliosphere was examined by *Meng et al.* (2015).

3.8 Enabling More Efficient Execution

Efficient execution becomes even more critical in enabling routine use of the most complex MHD models in a near real time operational environment. Improving time to solution is both a software and hardware challenge. Smarter AMR algorithms can focus computational effort where it is most effective. Porting algorithms to faster GPU chips can make best use of recent hardware developments.

3.8.1 Adaptive Mesh Techniques to Support Efficient High Resolution Models

Adaptive Mesh Refinement allows models to focus the computational effort at points in the solution that require the most spatial resolution. For models of the ambient solar wind, this capability is most relevant in the lower coronal section of the combined model. As the MHD models of the coronal field evolve to include more detailed representations of fine structure within active regions and embedded flux ropes, AMR will be essential to achieve reasonable time-to-solution. A number of models already include the ability to adaptively refine the mesh or use fixed meshes that have higher resolution at pre-identified locations. The SWMF was developed with a cartesian block adaptive foundation (*Toth et al.* (2012)). Both the AMR SIP-CESE Solar Wind Model (*Feng et al.* (2012)) and ENLIL (*Odstrcil* (2003),*Odstrcil et al.* (2003)) can use the PARAMESH AMR package (*MacNeice et al.* (2011)). The CORHEL suite can use a fixed mesh which variable spacing which concentrates mesh points at desired locations (e.g. *Mok et al.* (2016)).

3.8.2 Porting Codes to GPUs

Inevitably, as physics based models evolve to include additional physical processes and more complex field topologies, and are required to execute in ensemble mode, they become more expensive to run. This poses a computational resource challenge to oper-

728 ational centers. Traditionally this meant investing in large expensive computational sys-

729 tems or farming out model runs to remote supercomputers, which can lead to issues with

730 accessibility, data transfer speeds, and guarantees of acceptable time to solution.

731 Recently, accelerated computing using Graphics Processing Unit (GPU) technol-

732 ogy has become a viable alternative to traditional multicore systems. GPUs can offer

733 economical computation that is equivalent to hundreds or thousands of cores on tradi-

734 tional systems. They also allow facilities the planning flexibility to make small incremen-

735 tal increases to their computing power at low cost.

736 A number of developers of space weather models have already explored the use of

737 GPUs (*Germaschewski and Raeder* (2011)). These early adopters needed major code rewrites

738 to port their codes to the GPUs. The cost of developing a GPU version of their code while

739 also maintaining and developing the existing code discouraged others from following this

740 lead. Recent software developments have removed this impediment.

741 The OpenACC 2.0 standard (https://www.openacc.org) was established in 2013

742 (the current standard is OpenACC 2.6), and has opened the door for legacy codes to take

743 advantage of GPU acceleration while maintaining compatibility with standard architec-

744 tures. OpenACC allows the use of compiler directives that appear as comments in FOR-

745 TRAN or C/C++ code. These directives identify portions of the code for acceleration,

746 similar to the OpenMP standard. It offers a powerful set of constructs to accelerate com-

747 putations on GPUs, while maintaining compatibility with existing MPI implementations.

748 The PSI group is now modifying the CORHEL suite to leverage these software de-

749 velopments (*Caplan et al.* (2017)), and if successful, would point the way for all other

750 existing models to achieve similar performance boosts.

4 Model Inputs - Problems and Prospects

4.1 Magnetogram Issues

753 The ambient solar wind model solutions are determined, in large part, by the sur-

754 face magnetic field information which sets the lower boundary conditions of the coro-

755 nal field model. Almost all of the models of the ambient corona that have been used to

756 drive solar wind models have used Line-Of-Sight (LOS) magnetograms. There are a num-

757 ber of well documented problems with these magnetograms.

1. Magnetograms from different observatories give fields with different amplitudes, amounting in some cases to factors as large as 4 (*Riley et al.* (1969)).

2. Magnetograph measurements are computed assuming a spatially constant magnetic field and uniform atmosphere over a given detector pixel. In reality this assumption is never satisfied the data are at best averages over unknown sub-resolution field structures, with response functions that vary depending on spectral and spatial resolution and integration time. Magnetogram calibration is dependent on polarimetric models to account for these spectral, spatial, and temporal resolution shortcomings. This can introduce significant differences to the 'observed' flux levels (*Leka and Barnes* (2012)), and ultimately impact solar wind models.

3. Interpolation and rebinning when combining individual full disk magnetograms into synoptic maps can add further error, principally due to the temporal averaging of the time varying field. *Pevtsov et al.* (2015) analyzed this by developing variance estimates (*Bertello et al.* (2014)) for the NSO/SOLIS synoptic magnetograms and used them in ensemble mode to study their impact on the forecasts of the WSA/ENLIL model for L1. They estimated that the location of the HCS and photospheric neutral line could vary by as much as 5° in the PFSS solution and that that error was propagated into the WSA/ENLIL wind solutions.

4. Polar fields are poorly measured. Because of the tilt of the Earth's orbit, the poles are alternately obscured producing data gaps. Also the polar fields are mostly radial leading to low signal to noise in LOS measurements. Both issues are usually managed using interpolation of fields from lower latitudes. Polar fields are critically important for determining the large scale coronal magnetic field, as they affect the lower degree harmonics disproportionately.

5. Field measurements are only trusted from near disk center.

6. Most LOS instruments calculate radial fields by simply dividing the full-disk LOS field data by the cosine of the angle between the LOS and the solar surface normal. This procedure is generally accurate in weaker field regions where the true field is approximately radial but it breaks down in sunspot active regions (*Leka et al.* (2017)) and can cause serious errors in coronal field models, particularly in the topology of the HCS.

7. Global models require global surface fields provided through synoptic magnetograms. These synoptic magnetograms are constructed using measurements made within

791   60 degrees longitude of disk center and used in global models under the assump-

792   tion that the field does not change as the sun rotates. This is of course not true.

793   *Arge et al.* (2013) have shown that active regions emerging on the far-side mod-

794   ify the global solution enough to influence the solution on the near side.

795   8. Magnetograms are not uniformly sensitive to different levels of magnetic flux.

796   In addition, as shown by *Toth et al.* (2011), care must be taken when using poten-

797   tial field solvers based on spherical harmonic expansion, because of convergence issues

798   associated with the near polar values of higher order harmonics. For this reason they rec-

799   ommend using finite difference based solvers.

800   As we mentioned above in 3.3, the models consistently underestimate the amount

801   of open flux in the heliosphere. Given these issues with the magnetograms that is hardly

802   surprising.

803   Some of these deficiencies will be addressed through adoption of assimilative sur-

804   face flux transport models of the solar field such as ADAPT, SURF or AFT (see 4.2).

805   Some may be addressed by adopting more complete vector magnetogram datasets. It

806   should be noted that vector data has some issues of its own.

807   1. The LOS component of vector field data is significantly less noisy than the hor-

808   izontal components.

809   2. Disambiguation of the vector field direction has to be imposed

810   3. The most complete of these datasets, from SDO/HMI, has an orbital signature

811   which has yet to be properly characterized.

4.2 Surface Field Models

813   Many of the deficiencies of the synoptic magnetograms discussed in 4.1 will be ad-

814   dressed through assimilative modeling of the evolving surface flux. Models such as ADAPT

815   (*Arge et al.* (2010), *Hickmann et al.* (2015)), SURF, AFT (*Upton and Hathaway* (2014)),

816   ESFTM (*Schrijver and De Rose* (2003)) and others (e.g. *Cameron et al.* (2010)) do this.

817   ADAPT, for example, develops an ensemble of simulations of the time evolution of the

818   surface flux using the Worden and Harvey model (*Worden and Harvey* (2000)), which

819   includes the influence of differential rotation, meridional flow, super-granular diffusion,

820   and random emergence of weak background flux. The Los Alamos National Laboratory

Ensemble Kalman Filter (ENKF) data-assimilation method is used to adjust the ADAPT model as new observational data becomes available. ADAPT maps are now routinely posted to the web, and coronal and solar wind models are beginning to use these as inputs (*Merkin et al.* (2016),*Linker et al.* (2016), *Linker et al.* (2017)). The SURF model has been delivered to the CCMC and is being tested and configured for operation.

Preliminary testing of the models with ADAPT maps (*Linker et al.* (2016)) does not yet show any marked improvement over results from the old static maps, but considerable re-calibration and tuning of the WSA still needs to be done before comprehensive validation studies can be executed. When run in near real time, the leading polarity spots appear first in the ADAPT maps when an active region rotates around the east limb, and this can lead to an overall imbalance of positive and negative flux. Techniques to rebalance the flux are currently being investigated. In addition, these newly rotated east limb ARs may have appeared a few days earlier on the far side, but can only be assimilated into the time dependent map realizations once they are observed. This forced 'catch-up' can lead to errors in the global fields temporal evolution.

5 Research Topics Not Yet in Ambient Wind Models

5.1 Parameterization of Sub-Scale Processes

Sub-scale physical processes affect the ambient wind solution in two ways. The first is through ubiquitous 'volumetric' source terms in the MHD equations which are really determined by kinetic processes. The obvious example would be the local heating and acceleration rates due to dissipation of fine scale alfvenic turbulence which is discussed in 3.6 and 5.2. It would also include the rates of exchange of thermal energy and momentum between ions and electrons which are known to have different temperatures and different degrees of thermal anisotropy, resulting perhaps in the development of instabilities such as firehose and mirror (*Kasper et al.* (2006)).

The second way is through the sensitivity of the large scale solution to sub-scale processes at critical locations. The obvious example of this would be the way sub-scale processes set the true plasma resistivity and reconnection rates in the centers of current sheets. Classical estimates of the plasma resistivity in the corona and heliosphere are very low and so in practice in MHD codes this is always overwhelmed by numerical resistivity due to the finite resolution of the models. The true reconnection rates are determined

852 by sub-grid scale kinetic physics. Particle codes and Hall-MHD codes are being used to

853 study reconnection in these small scale regimes. Although the physical reconnection pro-

854 cess occurs at the small scales, there is both observational and modeling evidence to sug-

855 gest that the effective large scale reconnection rates are actually determined, through

856 non-linear small scale evolution, by the macro-scale conditions (*Cassak et al.* (2017)).

857 Studies are in progress to understand how to use these insights to control local resistiv-

858 ity in global MHD models, but it may be at least a decade before this is propagated for-

859 ward into operational forecast models. These improvements will have a significant im-

860 pact on MHD models of evolving coronal structure, on the nature of the HCS and the

861 ability of the models to forecast B_z[1].

5.2 Time Dependence of the Solar Wind

863 The solar wind is unsteady but its temporal evolution is still not well understood.

864 It is instructive to consider the wind time dependence as a function of spatial scales in

865 order to appreciate which aspects of the wind's time dependence may be better addressed

866 by the MHD models in the near future.

867 At larger spatial scales ($> 10^5$ km) the ambient fast wind is relatively steady and

868 the disturbances that do exist are small amplitude. At the finest scales ($< 10^2$ km) alfvenic

869 turbulence is observed, primarily propagating outward, and is believed to contribute to

870 both heating and accelerating the wind. Between these scales, in what is known as the

871 inertial range, the non-linearity of the MHD equations causes some of the energy in the

872 larger scale disturbances to cascade to finer scales as the disturbances propagate outward.

873 If and when this energy reaches the ion spatial scale it can be dissipated (e.g. *Kiyani et*

874 *al.* (2015)). A key question is, at a given point in the wind, how much of the local alfven

875 wave flux is the result of injection and propagation from the sun and how much is due

876 to coarser disturbances near the sun cascading to finer scales in transit from the sun?

877 Observations do not currently answer this question.

878 For MHD models of the fast wind in the ambient heliosphere, given current com-

879 putational limitations, only the coarsest section of the inertial range is likely to be re-

880 solved in the next decade. Nevertheless, together with in situ observations from the Parker

---

[1] B_z is essentially the same as the RTN coordinate component B_N.

881   Solar Probe, successfully reproducing this section of the inertial range spectrum would

882   determine the correct statistical description of coarser disturbances affecting the fast wind.

883   It would then enable modelers to understand the role of specific processes such as the

884   Kelvin-Helmholtz instability in the cascade. At the finest scales, more accurate charac-

885   terization of the amplitude of fine scale turbulence will define how the boundary fluxes

886   and source terms for the alfven wave heating equations (see 3.6) should be set.

887   In contrast to the fast wind, the slow wind is unsteady with large amplitude fluc-

888   tuations at all scales. The source of the slow wind is controversial. While everything we

889   noted about the fast wind also applies to the slow wind, in addition the slow wind's large

890   amplitude fluctuations at the coarsest scale require that we understand the coronal struc-

891   tures that drive these. The slow solar wind is typically found surrounding the HCS and

892   appears to have abundances similar to that of the closed corona. It appears to originate

893   from a number of different coronal features (e.g. *Cranmer et al.* (2017)).

894   A significant component of the slow wind clearly comes from larger structures formed

895   by the boundaries of coronal holes and the outermost fieldlines of the streamers formed

896   by the neighboring regions of closed field. Helmet streamers are not in equilibrium and

897   their outer-most closed fieldlines undergo periods of expansion and pinch-off through mag-

898   netic reconnection, releasing 'blobs' of coronal plasma into the wind. These 'blobs' are

899   released intermittently at intervals ranging from hours for smaller blobs to tens of hours

900   for larger ones (e.g. *Viall and Vourlidas* (2015). The open fieldlines adjacent to pseudo-

901   streamers have more complex topologies but are also believed to contribute to the slow

902   wind.

903   In the photosphere all open fieldlines are close to closed loops that comprise the

904   magnetic carpet and it has been suggested that some of the slow wind is transferred from

905   the closed carpet fieldlines to the open fieldlines through a constant process of local mag-

906   netic reconnection (e.g. *Cranmer* (2018)). Finally the The S-web concept can encom-

907   pass all of these ideas. It postulates that the slow wind originates from a network of nar-

908   row open-field corridors which map to a web of separatrices and quasi-separatrix layers

909   in the heliosphere (*Antiochos et al.* (2011)).

910   SIRs represent the boundary between the fast and slow wind, and when the Sun

911   is active, up to 50% of SIRs can be transient, indicating they vary much within one so-

912   lar rotation (*Jian et al.* (2006)).

Improving models of the coarse scale slow wind structure will require using time dependent high resolution models of the corona driven by high cadence vector magnetograms (see 3.5 and 4.2). At present modeling of these slow wind source region theories is still restricted to idealized scenarios, and techniques to drive MHD codes using time varying photospheric vector fields are still in the earliest stages of their development. We anticipate that it will take a decade before models of the streamer related and S-web sources will be mature enough, and computational platforms sufficiently powerful to support routine use in MHD forecasting models. The inclusion of slow wind sources associated with interchange reconnection between open field and closed magnetic carpet fieldlines may require significantly more resolution and would likely only be included in the next decade through some form of statistical parameterization.

5.3 Tomography Data

The physics behind the UCSD kinematic tomographic modeling becomes inadequate when used near the Sun, in regions very distant from it, or when exploring shock processes. To eliminate this deficiency in the kinematic tomography the UCSD group has produced a tomographic analysis whereby the IPS analysis can iteratively update 3-D MHD models as a kernel in the IPS time dependent tomography. Used with both ENLIL and the MS-FLUKSS 3-D MHD modeling to date this process allows an iterative best fit of 3-D MHD models to IPS data rather than the provision of 3-D MHD forward modeling from a lower boundary.

The ENLIL hybrid process UCSD has developed begins by providing the 3-D MHD model with a kinematic model boundary. The IPS driven ENLIL model then outputs a first iteration volumetric matrix. The 3-D velocities and densities from this matrix are traced back to the source surface boundary and used with repeated boundary updates to the ENLIL model for an iterated solution best fit of the IPS data for velocity and density. By beginning a source surface with the kinematic modeling, inputs tests show that only three iterations are sufficient for a low resolution iterative ENLIL model convergence; this takes less than 6 hours of time on modest 8 node processors. While this technique provides better defined shock fronts, and non-radial plasma transport, this analysis has yet to be operated in real time (*Jackson et al.* (2018)).

Future versions of this analysis are expected to use current 3-D MHD initiation techniques, such as ENLIL with current cone model technology or even more sophisticated 3-D MHD models that begin near the solar surface. In this way these models can be iteratively corrected for values of density, velocity, and magnetic fields as heliospheric structures move outward from the Sun. Weighted preference can be given for those parameters and timing values that are the best known and resolved both near the surface and remotely.

Current IPS tomographic technology is low resolution, with possibilities of at most a few thousand lines-of-sight to scintillating radio sources per day, and the IPS analysis has ambiguities about the relationship between the proxy parameters for small scale density variations observed and bulk density. This is not the same for heliospheric imagers that view Thomson scattering from heliospheric electrons (*Jackson et al.* (2004)), and since the middle of the first decade of this century the CCMC has also hosted the Solar Mass Ejection Imager (SMEI) tomographic analysis at Runs on Request. Heliospheric imagers provide LOS measurements of as many as several hundreds of thousand per day, and tomographic resolutions in 3-D potentially commensurate with the cube root of these numbers. Updates of similar tomographic systems to SMEI are currently planned that include a NASA Small Explorer Mission scientific mission now in Phase A, the Polarimeter to Unify the Corona and Heliosphere (PUNCH), and a recently funded NASA operational mission concept, the All-Sky Heliospheric Imager (ASHI). Both missions promote the extant SMEI tomographic system and updates to this system including a 3-D MHD analysis kernel for use in their proposed concept studies.

6 Conclusions

In this review we have assessed two types of models. The first type aims to use analytical/empirical relations, with the help of statistics and optimization to obtain the best prediction for the solar wind at the L1 point. The second type, the MHD models, use first-principle, physics-based forward modeling.

From an operational forecast perspective, for the limited set of parameters which they report (excepting B_z), empirical models such as AnEn, PROJECTZED and PDF currently outperform semi-empirical models like WSA which in turn matches or beats the MHD models. The limited validation data for the IPS based tomographic model Hel-

Tomo suggest that it achieves performance between that of the empirical and WSA model. The MHD models reproduce the interplanetary magnetic sector structure reasonably well, but all MHD models underestimate the global open flux by about a factor of 2. For wind properties at L1, the wind speed is the most reliable forecast followed by that of particle number density. Both plasma temperature and B_z are very poorly reproduced.

One might ask, 'why do we need the expensive MHD models at all if the cheaper empirical models predict the solar wind to the same level or better?' The answer is, of course, that the cheaper models provide only partial information about the solar wind, while the MHD models offer insight into the underlying physics which we are trying to understand.

The pattern matching models beat all others in part because they use the L1 observations directly, while both WSA and MHD models use photospheric magnetogram data with significantly greater errors associated with both measurement and interpretation. Of course the empirical models do not support forecasting at locations other than L1, and offer relatively little scientific insight.

While not the focus of the present study, the pattern matching approaches also provide little scope for forecasting transient solar wind structures prior to their arrival at L1. In principle, once the leading edge of a transient structure has passed L1, pattern matching could provide a short-lead-time ($<$ 24 hours) forecast of remaining structure (e.g., *Chen et al.* (1997)), providing the historic solar wind record contains enough suitable analogues.

We anticipate that the near realtime forecasts for both WSA and the MHD models will improve to match that of the empirical models, through the use of two approaches to intelligent pre-conditioning. With the use of ADAPT maps, an ensemble of at least 12 WSA related models evolutions will be available. By comparing the WSA ADAPT forecasts to those of the empirical models, it should be possible to identify the best choice for the immediate forecast window, and then submit these to the more computationally expensive MHD models. In addition, the pre-conditioning of the MHD solutions using the IPS tomography models will force the solution toward the observed wind state. Both of these pre-conditioning approaches are currently in development, and should close the gap in forecast quality between the empirical and physics based models. These devel-

opments will not improve the L1 forecast beyond that of the empirical models, but it should improve the model solution at other points in the heliosphere.

The MHD models have made great advances in recent years in supporting scientific research. More complete descriptions of the important physical process have been added, advances have been made in understanding how to craft and process time dependent photospheric magnetic field maps, and the coronal field models have demonstrated the ability to model increasingly complex field topologies. The success of the July 2017 eclipse forecast in reproducing the observed complex coronal topology illustrates this. These new capabilities are still limited to scientific studies, but most can be expected to migrate into operational codes during the next decade.

The ability to accommodate more complex field topologies in the coronal MHD models, together with the use of high cadence and high resolution photospheric magnetic vector field observations to drive the models, offers the prospect, for the first time, of realistically representing the time dependence of the coarser scale features in the ambient wind. An obvious example would be the larger plasma blobs released aperiodically from the tips of helmet streamers. Progress in representing finer scales will require improvements in the resolution and cadence of the observations used to drive the models.

We anticipate that in-situ observations of the turbulence spectrum, including new near sun data from the Parker Solar Probe, will better inform how wave dissipation and other mechanisms are tuned to define local heating and acceleration.

The ever increasing sophistication and physical realism of the models will support a wealth of new scientific insights. However this will not necessarily translate into improved operational forecast quality. An obvious question to pose is 'when will the physics based models outperform the empirical models?'. The case can be made that advances in model design have positioned the models to achieve this over the next decade. However the pace of their development has outstripped the pace of improvements in the quality of the input data which they consume, and until this is remedied, these models will not achieve their full forecasting potential.

References

Altschuler,M.D. and Newkirk,G. (1969), Magnetic Fields and the Structure of the Solar Corona. I: Methods of Calculating Coronal Fields, *Solar Phys.*, **9**, 131, doi:10.1007/BF00145734

Aly,J.J., (1989), *Solar Phys.*, On the reconstruction of the nonlinear force-free coronal magnetic field from boundary data, **120**, 19, doi:10.1007/BF00148533

Amari,T., Aly,J.J., Luciani,J.F., Boulmezaoud,T.Z. and Mikic,Z., (1997), Reconstructing the solar coronal magnetic field as a force free magnetic field, *Solar Phys.*, **174**, 129, doi:10.1023/A:1004966830232

Antiochos,S.K., Mikic,Z., Titov,V.S., Lionello,R. and Linker,J.A., (2011), A Model for the Sources of the Slow Solar Wind, *Astrophys.J.*, **731**, 112, doi:10.1088/0004-637X/731/2/112

Arge,C.N. and Pizzo,V.J., (2000), Improvement in the prediction of solar wind conditions using near-real time solar magnetic field updates,*J. Geophys. Res.*, 105(A5), 10465, doi:10.1029/1999JA000262

Arge,C.N., Henney,C.J., Koller,J., Compeau,C.R., Young,S., MacKenzie,D., Fay,A. and Harvey,J.W, (2010), Air Force Data Assimilative Photospheric Flux Transport (ADAPT) Model, *AIP Conference Proceedings*, **1216**, 343, https://doi.org/10.1063/1.3395870

Arge,C.N., Henney,C.J., Gonzalez Hernandez,I., Toussaint,W.A., Koller,J. and Godinez,H.C. (2013), Modeling the Corona and Solar Wind using ADAPT Maps that Include Far-Side Observations *Solar Wind 13 : AIP Conference Proceedings*, **1539**, 11, doi:10.1063/1.4810977

Bertello,L., Pevtsov,A.A., Petrie,G.J.D. and Keys,D., 2014. Uncertainties in solar synoptic magnetic flux maps. *Solar Phys.*, **289**, 2419, doi:10.1007/s11207-014-0480-3

Bussy-Virat,C.D. and Ridley,A.J., (2014), Predictions of the solar wind speed by the probability distribution function model, *Space Weather*, **12**, 337, doi:10.1002/2014SW001051

Bussy-Virat,C.D. and Ridley,A.J., (2016), Twenty-four hour predictions of the solar wind speed peaks by the probability distribution function model, *Space Weather*, **14**, 861, doi:10.1002/2016SW001437

Cameron,R.H., Jiang,J., Schmitt,D. and Schussler,M., (2010), Surface Flux Transport Modeling for Solar Cycles 15-21: Effects of Cycle Dependent Tilt Angles of Sunspot Groups, *Astrophys.J.*, **719**, 264, doi:10.1088/0004-637X/719/1/264

Caplan,R., Linker,J. and Mikic,Z., (2017), *presented at the NVIDIA GPU Technology Conference*, http://on-demand.gputechconf.com/gtc/2017/video/s7535-ronald-caplan-potential- field-solutions-of-the-solar-corona-converting-a-pcg-solver-from-mpi-to- mpi+openacc.mp4.

Cassak,P.A., Liu,Y.-H. and Shay.M.A., (2017), A review of the 0.1 reconnection rate problem, *J.Plasma Phys.*,**83**, 715830501, doi:10.1017/S0022377817000666

Chandran,B.D.G., Dennis,T.J., Quataert,E. and Bale,S.D., (2011), Incorporating Kinetic Physics into a Two-fluid Solar-wind Model with Temperature Anisotropy and Low-frequency Alfven-wave Turbulence, *Astrophys.J.*, **743**, 197, doi:10.1088/0004-637X/743/2/197

Chapman,S. and Bartels,J., (1940), *Geomagnetism*, Oxford University Press, London.

Chen,J., Cargill,P.J. and Palmadesso,P.J., (1997), Predicting solar wind structures and their geoeffectiveness, *J. Geophys. Res.*, **102**(A7), 14701, doi: 10.1029/97JA00936

Chifu,I., Wiegelmann,T. and Inhester,B., (2017), Nonlinear Force-free Coronal Magnetic Stereoscopy, *Astrophys.J.*, **837**, 10, 10.3847/1538-4357/aa5b9a

Cohen,O., (2017), A Comparison between Physics-based and Polytropic MHD Models for Stellar Coronae and Stellar Winds of Solar Analogs, *Astrophys.J.*, **835**, 220, doi:10.3847/1538-4357/835/2/220

Cranmer,S.R., Gibson,S.E. and Riley,P., (2017), Origins of the Ambient Solar Wind: Implications for Space Weather, *Space Sci. Rev.*, **212**, 1345, doi:10.1007/s11214-017-0416-y

Cranmer,S.R , (2018), Low-frequency Alfven Waves Produced by magnetic Reconnection in the Sun's Magnetic Carpet, *Astrophys. J.*.**862**, 6, doi:10.3847/1538-4357/aac953

Den,M., Tanaka,T., Kubo,Y. and Watari,S. (2015), Three-dimensional MHD simulation of the solar wind from the solar surface to 400 solar radius using REPPU (REProduce Plasma Universe) code, Proceedings of the 34th International Cosmic Ray Conference (ICRC2015). 30 July - 6 August, 2015. The Hague, The Netherlands.

DeRosa,M.L., Schrijver,C.J., Barnes,G., Leka,K.D., Lites,B.W., Aschwanden,M.J., Amari,T., Canou,A., McTiernan,J.M., Regnier,S., Thalmann,J.K., Valori,G., Wheatland,M.S., Wiegelmann,T., Cheung,M.C.M., Conlon,P.A., Fuhrmann,M., Inhester,B. and Tadesse,T (2009), A critical assessment of nonlinear force free field modeling of the solar corona for active region 10953 *Astrophys. J.*, **696**, 1780, doi:10.1088/0004-637X/696/2/1780

DeRosa,M.L., Wheatland,M.S., Leka,K.D., Barnes,G., Amari,T., Canou,A., Gilchrist,S.A., Thalmann,J.K., Valori,G., Wiegelmann,T., Schrijver,C.J., Malanushenko,A., Sun,X. and Regnier,S., (2015), The Influence of Spatial resolution on Nonlinear Force-free Modeling, *Astrophys.J.*, **811**, 107, doi:10.1088/0004-637X/811/2/107

Detman,T., Smith,Z., Dryer,M., Fry,C.D., Arge,C.N. and Pizzo,V., (2006) A hybrid heliospheric modeling system: Background solar wind, *J. Geophys. Res.*, **111**, A07102, doi:10.1029/2005JA011430

Downs,C., Roussev,I.I.,, van der Holst,B., Lugaz,N., Sokolov,I.V. and Gombosi,T.I. (2010), *Astrophys.J.*, **712**, 1219, doi:10.1088/0004-637X/712/2/1219

Downs,C., Lionello,R., Mikic,Z., Linker,J.A. and Velli,M., (2016), Closed-field Coronal Heating Driven by Wave Turbulence, *Astrophys.J.*, **832**, 180, doi:10.1088/0004-637X/832/2/180

Dunn,T., Jackson,B.V., Hick,P.P., Buffington,A. and Zhao,X.P., (2005), Comparative Analyses of the CSSS Calculation in the UCSD Tomographic Solar Observations, *Solar Phys.*, **227**, 339, doi:10.1007/s11207-005-2759-x

1129   ESWF, (2018), http://swe.uni-graz.at/index.php/services/solar-wind-forecast.

1130   Echer,E., Korth,A., Bolzan,M.J.A. and Freidel,R.H.W., (2017), Global ge-

1131   omagnetic responses to the IMF B_z fluctuations during the Septem-

1132   ber/October 2003 high speed stream intervals, *Ann. Geophys.*, **35**, 853,

1133   https://doi.org/10.5194/angeo-35-853-2017

1134   Feng,X., Yang,L., Xiang,C., Jiang,C., Ma,X., Wu,S.T., Zhong,D. and Zhou,Y.,

1135   (2012), Validation of the 3D AMR SIPCESE Solar Wind Model for Four Car-

1136   rington Rotations, *Solar Phys.*, **279**, 207, doi:10.1007/s11207-012-9969-9

1137   Feng,X., Li,C., Xiang,C., Zhang,M., Li,H. and Wei,F., (2017) Data-driven Mod-

1138   eling of the Solar Corona by a New Three-dimensional Path-conservative

1139   OsherSolomon MHD Model, *Astrophys.J.Suppl.*,**233**,10, doi:10.3847/1538-

1140   4365/aa957a

1141   Fisher,G.H., Welsch,B.T., Abbett,W.P. and Bercik,D.J., (2010), Estimating elec-

1142   tric elds from vector magnetogram sequences, *Astrophys. J.*, **715**, 242,

1143   doi:10.1088/0004-637X/715/2/242

1144   Fisher,G.H., Welsch,B.T. and Abbett,W.P., (2012), Can we determine electric fields

1145   and Poynting fluxes from vector magnetograms and doppler measurements?,

1146   *Solar Phys.*, **277**, 153, doi:10.1007/s11207-011-9816-4

1147   Fisher,G.H., et al. (2015), The CoronalGlobal Evolutionary Model: Using

1148   HMI Vector Magnetogram and Doppler Data to Model the Buildup of

1149   Free Magnetic Energy in the Solar Corona, *Space Weather*, **13**, 369,

1150   doi:10.1002/2015SW001191

1151   Fry,C.D., Sun,W., Deehr,C.S., Dryer,M., Smith,Z., Akasofu,S-I., Tokumaru,M. and

1152   Kojima,M., (2001), Improvements to the HAF solar wind model for space

1153   weather predictions,*J. Geophys. Res.*, **106**, 20985, doi:10.1029/2000JA000220

1154   Gary,G.A., (2001), Plasma beta above a solar active region: rethinking the

1155   paradigm, *Solar Phys.*, **203**, 71, doi:10.1023/A:1012722021820

1156   Gauss,C.F., (1839), AllgemeineTheorie des Erdmagnetismus, Resultate aus den

1157   Beobachtungen des magnetischen Vereins im Jahre 1838, 1.

1158   Germaschewski,K. and Raeder,J. (2011). Using Automated Code Generation to

1159   Support High Performance Extended MHD Integration in OpenGGCM. *ASP*

1160   *Conf. Ser.*, **444**, 197.

Gibson,S., Kucera,T., White,S., Dove,J., Fan,Y., Forland,B., Rachmeler,L.,
Downs,C. and Reeves,K. (2016), FORWARD: A toolset for multiwavelength
coronal magnetometry, *Frontiers in Astronomy and Space Sciences*, **3**, 8,
doi:10.3389/fspas.2016.00008

Gombosi, T. I., De Zeeuw,D.L., Groth,C.P., Powell,K.G., Clauer,C.R. and Song,P.,
(2001), *From Sun to Earth: Multiscale MHD simulations of space weather, in
Space Weather, Geophys. Monogr. Ser.*, **125**, edited by P. Song, H. J. Singer,
and G. L. Siscoe, pp. 169176, AGU, Washington, D.C.

Gressl,C., Veronig,A. M.,Temmer,M., Odstrcil,D., Linker,J. A., Mikic,Z. and Ri-
ley,P., (2014), Comparative Study of MHD Modeling of the Background Solar
Wind *Solar Phys.*, **289**, 1783, doi:10.1007/s11207-013-0421-6

Hayashi,K., (2012), An MHD simulation model of time-dependent co-
rotating solar wind, *J. Geophys. Res. Space Physics*, **117**, A08105,
doi:10.1029/2011JA017490

Hayashi,K. (2013), An MHD simulation model of time-dependent global solar corona
with temporally varying solar-surface magnetic field maps, *J. Geophys. Res.
Space Physics*, **118**, 6889, doi:10.1002/2013JA018991

Hayashi,K., Feng,X., Xiong,M. and Chaowei Jiang,C., (2018), An MHD Simulation
of Solar Active Region 11158 Driven with a Time-dependent Electric Field De-
termined from HMI Vector Magnetic Field Measurement Data, *Astrophys.J.*,
855, 11, 10.1088/0004-637X/855/2/11

Hickmann,K.S., Godinez,H.C., Henney,C.J. and Arge,C.N., (2015), Data assimilation
in the ADAPT photospheric flux transport model, *Solar Phys.*, **290(4)**, 1105,
doi:10.1007/s11207-015-0666-3

Jackson,B.V., Hick,P.L., Kojima,M. and Yokobe,A., (1998) Heliospheric tomogra-
phy using interplanetary scintillation observations 1. Combined Nagoya and
Cambridge data *J. Geophys. Res.*, **103**, 12049, doi:10.1029/97JA02528

Jackson,B.V., Hick,P.P. and Buffington,A., (2002), Time-Dependent Tomography of
Heliospheric Features Using Interplanetary Scintillation (IPS) Remote-Sensing
Observations, *Solar Wind 10 Conference Proceedings, Pisa, June 17-21*, 31.

Jackson,B.V., Buffington,A., Hick,P.P., Altrock,R.C., Figueroa,S., Holladay,P.E.,
Johnston,J.C., Kahler,S.W., Mozer,J.B., Price,S., Radick,R.R., Sagalyn,R.,
Sinclair,D., Simnett,G.M., Eyles,C.J., Cooke,M.P., Tappin,S.J., Kuchar,T.,

Mizuno,D., Webb,D.F., Anderson,P. A., Keil,S.L., Gold,R.E. and Waltham,N. , (2004) , The Solar Mass-Ejection Imager (SMEI) Mission, *Solar Phys.*, **225**, 177, doi:10.1007/s11207-004-2766-3

Jackson,B.V., Hick,P.P., Bisi,M.M., Clover,J.M. and Buffington,A., (2010), Inclusion of In-Situ Velocity Measurements into the UCSD TimeDependent Tomography to Constrain and Better Forecast Remote Sensing Observations, *Solar Phys.*, **265**, 245, doi:10.1007/s11207-010-9529-0

Jackson,B.V., Hick,P.P., Buffington,A., Bisi,M.M., Clover,J.M., Tokumaru,M., Kojima,M. and Fujiki,K., (2011), Three-dimensional reconstruction of heliospheric structure using iterative tomography: A review, *Journal of Atmospheric and Solar-Terrestrial Physics*, **73**, 1214, doi:10.1016/j.jastp.2010

Jackson,B.V., Clover,J.M., Hick,P.P., Buffington,A., Bisi,M.M. and Tokumaru,M., (2013), Inclusion of Real-Time In-Situ Measurements into the UCSD Time-Dependent Tomography and Its Use as a Forecast Algorithm, *Solar Phys.*, **285**, 151, doi:10.1007/s11207-012-0102-x

Jackson,B.V., Odstrcil,D., Yu,H-S., Hick,P.P., Buffington,A., Mejia-Ambriz,J.C., Kim,J., Hong,S., Kim ,Y., Han,J. and Tokumaru,M., (2015) The UCSD kinematic IPS solar wind boundary and its use in the ENLIL 3D MHD prediction model, *Space Weather*, **13(2)**, SW001130, https://doi.org/10.1002/2014SW001130

Jackson,B.V., Yu,H.-S., Buffington,A., Hick,P.P., Nishimura,N., Nozaki,N. Tokumaru,M., Fujiki,K. and Hayashi, K., (2016), Exploration of solar photospheric magnetic field data sets using the tomography, *Space Weather*, **14(12)**, 1107, doi:10.1002/2016SW001481

Jackson,B.V., Yu,H.-S., Hick,P.P., Buffington, A., Odstrcil,D., Pogorelov,N. and Kim,T., (2018), Heliospheric Tomography Results Using 3-D MHD Kernels, Oral presentation at the CCMC Workshop, 23-27 April, College Park, MD.

Jian,L., Russell,C.T., Luhmann,J.G. and Skoug,R.M., (2006). Properties of Stream Interactions at One AU During 1995 2004, *Solar Phys.*, **239**, 337, doi:10.1007/s11207-006-0133-2

Jian,L., Russell,C.T., Luhmann,J.G., MacNeice,P.J., Odstrcil,D., Riley,P., Linker,J.A., Skoug,R.M. and Steinberg,J.T. (2011). Comparison of Observations at ACE and Ulysses with Enlil Model Results: Stream Interaction

Regions During Carrington Rotations 2016 - 2018. *Solar Phys.*, **273**, 179–203, doi:10.1007/s11207-011-9858-7

Jian,L.K., MacNeice,P.J., Taktakishvili,A., Odstrcil,D., Jackson,B., Yu,H.-S., Riley,P., Sokolov,I.V. and Evans,R.M., (2015), Validation for solar wind prediction at Earth: Comparison of coronal and heliospheric models installed at the CCMC, *Space Weather*, **13**, 316, https://doi.org/10.1002/2015SW001174

Jian,L.K., MacNeice,P. J., Mays,M. L., Taktakishvili,A., Odstrcil,D., Jackson,B., Yu,H.-S., Riley,P. and Sokolov,I.V., (2016) Validation for global solar wind prediction using Ulysses comparison: Multiple coronal and heliospheric models installed at the Community Coordinated Modeling Center, *Space Weather*, **14**, 592, https://doi.org/10.1002/2016SW001435

Jiang,C.W. and Feng,X.S. (2013), Extrapolation of the solar coronal magnetic field from SDO/HMI magnetogram by a CESE-MHD-NLFFF code. *Astrophys. J.*, **769**, 144, doi:10.1088/0004-637X/769/2/144

Jiang,C., Wu,S.T., Feng,X. and Hu,Q., (2016), *Nature Communications*, **7**, 11522, doi:10.1038/ncomms11522

Jin,M., Manchester,W.B., van der Holst,B., Sokolov,I., Toth,G., Mullinix,R.E.,Taktakishvili,A., Chulaki,A. and Gombosi,T.I., (2017), Data-constrained Coronal Mass Ejections in a Global Magnetohydrodynamics Model, *Astrophys.J.*, **834**, 173, doi:10.1088/0004-637X/834/2/173

Kasper,J.C., Lazarus,A.J., Steinberg,J.T., Ogilvie,K.W. and Szabo,A., (2006), Physics-based tests to identify the accuracy of solar wind ion measurements: A case study with the Wind Faraday Cups, *J.Geophys.Res.*, **111**, A03105, doi:10.1029/2005JA011442

Kazachenko,M.D., Fisher,G.H. and Welsch,B.T., (2014), A comprehensive method of estimating electric fields from vector magnetic field and Doppler measurements, *Astrophys. J.*, **795**, 17, doi:10.1088/0004-637X/795/2/17

Kim,T.K., Arge,C.N. and Pogorelov,N.V., A Time dependent Heliospheric Model Driven by Empirical Boundary Conditions, (2018), *Space Weather*, This issue.

Kiyani,K.H., Osman,K.T. and Chapman,S.C., (2015), Dissipation and heating in solar wind turbulence: from the macro to the micro and back again, *Phil.Trans. A.*, **373**, 2041, doi:10.1098/rsta.2014.0155

Leake,J.E., Linton,M.G. and Schuck,P., (2017), Testing the Accuracy of Data-driven MHD Simulations of Active Region Evolution, *Astrophys.J.*, **838**, 113, doi:10.1088/0004-637X/838/2/113

Leka,K.D. and Barnes,G., (2012), Modeling and Interpreting the Effects of Spatial Resolution on Solar Magnetic Field Maps, *Solar Phys.*, **277**, 89, doi:10.1007/s11207-011-9821-7

Leka,K.D., Barnes,G. and Wagner,E.L., (2017): Evaluation (and Improving) Estimates of the Solar Radial Magnetic Field Component from Line-of-Sight Magnetograms, *Solar Phys.*, **292**, 36, doi:10.1007/s11207-017-1057-8

Lee,C.O., Luhmann,J.G., Odstrcil,D., MacNeice,P.J., de Pater,I., Riley,P. and Arge,C.N. (2009), The solar wind at 1 AU during the declining phase of solar cycle 23: comparison of 3D numerical model results with observations, *Solar Phys.*, **254**, 155, doi:10.1007/s11207-008-9280-y

Lepri,S.T., Antiochos,S.K., Riley,P., Zhao,L. and Zurbuchen,T.H., (2008), Comparison of Heliospheric In Situ Data with the Quasi-steady Solar Wind Models, textitAstrophys.J., **674**, 1158, doi:10.1088/0004-637X/674/2/1185

Levine,R.H., Schulz,M. and Frazier,E.N. (1982), Simultion of the magnetic structure of the inner heliosphere by means of a non-spherical source surface, *Solar Phys.*, **77**, 363, doi:10.1007/BF00156118

Linker,J.A., Caplan,R.M. Downs,C., Lionello,R., Riley,P., Mikic,Z., Henney,C.J., Arge,C.N., Kim,T. and Pogorelov,N., (2016), An Empirically Driven Time-Dependent Model of the Solar Wind, *Jour. of Physics: Conf. Series*, **719**, 012012, doi:10.1088/1742-6596/719/1/012012

Linker,J.A.; Caplan,R.M., Downs,C., Riley,P., Mikic,Z., Lionello,R., Henney,C.J., Arge,C.N., Liu,Y., Derosa,M.L., Yeates,A.. and Owens,M.J., (2017), The Open Flux Problem , *Astrophys.J.*, **848**, 70L, doi:10.3847/1538-4357/aa8a70

Lionello,R., Linker,J.A. and Mikic,Z., (2001), Including the Transition Region in Models of the Large-Scale Solar Corona, *Astrophys.J.* ,**546**, 542, doi:10.1088/0004-637X/546/2/542

Lionello,R., Linker,J.A. and Mikic, Z., (2003), Three Dimensional Magnetohydrodynamics of the Solar Corona and the Solar Wind with Improved Energy Transport, *AIP Conference Proceedings*, **679**, 222, doi:10.1063/1.1618582

Lionello, R., Linker, J. A.. and Mikic, Z. (2009), Multispectral Emission of the Sun during the First Whole Sun Month: Magnetohydrodynamic Simulations, *Astrophys.J.*, *690*, 902, doi:10.1088/0004-637X/690/1/902

Lionello,R., Velli,M., Linker,J.A. and Mikic,Z., (2013), Integrating physics-based coronal heating and solar wind acceleration in a global MHD model, *AIP Conference Proceedings*, **1539**, 30, doi:10.1063/1.4810982

Lionello,R., Velli,M., Downs,C., Linker,J.A., Mikic,Z. and Verdini,A., (2014), Validating a Time-dependent Turbulence Drive Model of the Solar Wind, *Astrophys.J.*, **784**, 120, doi:10.1088/0004-637X/784/2/120

Lionello,R., Velli,M., Downs,C., Linker,J.A., Mikic,Z. and Verdini,A. , (2014) Validating a Time-dependent Turbulence-driven Model of the Solar Wind, *Astrophys.J.*, **784**, 120, doi:10.1088/0004-637X/784/2/120

Lionello,R., Velli,M., Downs,C., Linker,J. A. and Mikic,Z. (2014), Application of a Solar Wind Model Driven by Turbulence Dissipation to a 2D Magnetic Field Configuration, *Astrophys.J.*, **796**, 111, doi:10.1088/0004-637X/796/2/111

Lockwood,M., Owens,M.J., Barnard,L.A., Bentley,S., Scott,C.J. and Watt,C.E., (2016), On the Origins and timescales of geoeffective IMF, *Space Weather*, 14, 406, https://doi.org/10.1002/2016SW001375

Luhmann,J.G., Li,Y., Arge,C.N., Gazis,P.R. and Ulrich,R. (2002), Solar cycle changes in coronal holes and space weather cycles, *J. Geophys. Res.*, **107**, 1154, doi:10.1029/2001JA007550

Mackay,D.H. and van Ballegooijen,A.A., (2006), Models of the Large-Scale Corona. I. Formation, Evolution, and Liftoff of Magnetic Flux Ropes, *Astrophys. J.*, **641**, 577, doi:10.1088/0004-637X/641/2/577

MacNeice,P.J. (2009), Validation of community models: Identifying events in space weather model timelines, *Space Weather*, 7, S06004, doi:10.1029/2009SW000463

MacNeice,P.J. (2009), Validation of community models: 2. Development of a baseline using the Wang-Sheeley-Arge model, *Space Weather*, **7**, S12002, doi:10.1029/2009SW000489

MacNeice,P.J., Elliot,B. and Acebal,A. (2011), Validation of community models: 3. Tracing field lines in heliospheric models, *Space Weather*, **9**, S10003, doi:10.1029/2011SW000665

MacNeice,P., Olson,K.M., Mobarry,C., de Fainchtein,R. and Packer, C., (2011), PARAMESH V4.1: Parallel Adaptive Mesh Refinement, *Astrophysics Source Code Library*, ascl:1106.009

MacNeice,P. and Allred,J., (2018), MAGIC - MAGnetogram Interpolation and Composition, https://ccmc.gsfc.nasa.gov/support/MAGIC.

Malanushenko,A., Schrijver,C.J., DeRosa,M.L., Wheatland,M.S. and Gilchrist,S.A., (2012) Guiding Nonlinear Force-free Modeling Using Coronal Observations: First Results Using a Quasi-Grad-Rubin Scheme, *Astrophys.J.*, **756**, 153, doi:10.1088/0004-637X/756/2/153

Malanushenko,A., Schrijver,C.J., DeRosa,M.L. and Wheatland,M.S., (2014) Using Coronal Loops to Reconstruct the Magnetic Field of an Active Region before and after a Major Flare *Astrophys.J.*, **783**, 102, doi:10.1088/0004-637X/783/2/102

Meng,X., van der Holst,B., Toth,G. and Gombosi,T.I. (2015) Alfven wave solar model (AWSoM): proton temperature anisotropy and solar wind acceleration, *Monthly Notices of the Royal Astronomical Society*, **454**, 3697, doi:10.1093/mnras/stv2249

Merkin,V.G., Lyon,J.G., McGregor,S.L. and Pahud,D.M., (2011), Disruption of a heliospheric current sheet fold, *Geophys. Res. Lett.*, **38**, L14107, doi:10.1029/2011GL047822

Merkin,V.G., Lionello,R., Lyon,J.G., Linker,J., Torok,T. and Downs, C., Coupling of Coronal and Heliospheric Magnetohydrodynamic Models: Solution Comparisons and Verification, (2016), *Astrophys.J.*, **831**, 14, doi:10.1088/0004-637X/831/2/14

Metcalf,T.R., De Rosa,M.L., Schrijver,C.J., Barnes,G., van Ballegooijen,A.A., Wiegelmann,T., Wheatland,M.S., Valori,G. and McTiernan,J.M., (2008), Nonlinear Force-Free Modeling of Coronal Magnetic Fields. II. Modeling a Filament Arcade and Simulated Chromospheric and Photospheric Vector Fields, *Solar Phys.*, **247** , 269, doi:10.1007/s11207-007-9110-7

Mikic,Z, Linker,J.A., Schnack,D.D., Lionello,R. and Tarditi,A., (1999), Magnetohydrodynamic modeling of the global solar corona, *Physics of Plasmas*, **6**, 2217, doi:10.1063/1.873474

Mikic, Z., Linker,J.A., Lionello,R., Riley,P. and Titov,V. (2007). Predicting the Structure of the Solar Corona for the Total Solar Eclipse of March 29, 2006. In Demircan, O., Selam, S. O., and Albayrak, B., editors, Solar and Stellar Physics Through Eclipses, volume 370 of Astronomical Society of the Pacific Conference Series, page 299.

Mikic,Z., Downs,C., Linker,J.A., Caplan,R.M., Mackay,D.H., Upton,L.A., Riley,P., Lionello,R., Torok,T., Titov,V.S., Wijaya,J., Druckmuller,M., Pasachoff,J. M. and Carlos,W., (2018), Predicting the Corona for the 21 August 2017 Total Solar Eclipse *Nature Astronomy*, doi:10.1038/s41550-018-0562-5

Mok,Y., Mikic,Z., Lionello,R., Downs,C. and Linker,J.A., (2016), A Three-Dimensional Model of Active Region 7986: Comparison of Simulations With Observations, *Astrophys.J.*, **817**, 15, doi:10.1088/0004-637X/817/2/15

Nakamizo,A., Tanaka,T., Kubo,Y., Kamei,S., Shimazu,H. and Shinagawa,H., (2009), Development of the 3-D MHD model of the solar corona-solar wind combining system, *J.Geophys.Res.*,**114**, A07109, doi:10.1029/2008JA013844

Norquist,D.C. and Meeks,W.C., (2010), A comparative verification of forecasts from two operational solar wind models, *Space Weather*, **8**, S12005, doi:l0.1029/201OSW000598

Norquist,D.C. (2013), Forecast performance assessment of a kinematic and a magnetohydrodynamic solar wind model, *Space Weather*, **11** , 17, https://doi.org/10.1029/2012SW000853

Odstrcil,D., (2003), Modeling 3-D solar wind structure. *Advances in Space Research*, **32**, 497, doi:10.1016/S0273-1177(03)00332-6

Odstrcil,D., Vandas,M., Pizzo,V.J. and MacNeice,P., (2003) Numerical Simulation of Interacting Magnetic Flux Ropes, *AIP Conference Proceedings*, **679**, 699, doi:10.1063/1.1618690

Odstrcil,D., Pizzo,V.J., Linker,J.A., Riley,P., Lionello,R. and Mikic,Z., (2004) Initial coupling of coronal and heliospheric numerical magnetohydrodynamic codes, *Journal of Atmospheric and Solar-Terrestrial Physics*, **66**, 1311, doi:10.1016/j.jastp.2004.04.007

Oran,R., van der Holst,B., Landi,E., Jin,M., Sokolov,I.V. and Gombosi,T.I., (2013), A Global Wave-Driven Magnetohydrodynamic Solar Model With a Unified Treatment of Open and Closed Magnetic Field Topologies, *Astrophys.J.*, **778**,

176, doi:10.1088/0004-637X/778/2/176

Oran,R., Landi,E., van der Holst,B., Sokolov,I.V. and Gombosi,T.I, (2017), Alfven Wave Turbulence as a Coronal Heating Mechanism: Simultaneously Predicting the Heating Rate and the Wave-induced Emission Line Broadening, *Astrophys.J.*, **845**, 98, doi:10.1088/0004-637X/845/2/98

Owens,M.J., Arge,C.N., Spence,H.E. and Pembroke,A., (2005), An event based approach to validating solar wind speed predictions: High speed enhancements in the Wang-Sheeley-Arge model, *J. Geophys. Res.*, **110**, A12105, doi:10.1029/2005JA011343

Owens,M.J., Spence,H.E., McGregor,S., Hughes,W.J., Quinn,J.M., Arge,C.N., Riley,P., Linker,J. and Odstrcil,D., (2008), Metrics for solar wind prediction models: Comparison of empirical, hybrid, and physics-based schemes with 8 years of L1 observations, *Space Weather*, **6**, S08001, https://doi.org/10.1029/2007SW000380

Owens,M.J., Riley,P. and Horbury,T.S., (2017) Probabilistic Solar Wind and Geomagnetic Forecasting Using an Analogue Ensemble or 'Similar Day' Approach, *Solar Phys.*, **292**, 69, doi:10.1007/s11207-017-1090-7

Peter,H., Warnecke,J., Chitta,L.P. and Cameron,R.H., (2015), Limitations of force-free magnetic field extrapolations: Revisiting basic assumptions, *Astron. & Astrophys.*, **584**, A68, doi:10.1051/0004-6361/201527057

Pevtsov,A.A., Bertello,L. and MacNeice,P., (2015), Effect of uncertainties in solar synoptic magnetic flux maps in modeling of solar wind, *Advances in Space Research*, **56**, 2719, doi:10.1016/j.asr.2015.05.043

Pilot Results webpage, https://ccmc.gsfc.nasa.gov/challenges/SHINE/results.php. (2014).

Pizzo, V., Millward, G., Parsons, A., Biesecker, D., Hill, S. and Odstrcil, D., (2011), Wang-Sheeley-Arge-Enlil Cone Model Transitions to Operations, *Space Weather*, **9**, S03004, doi:10.1029/2011SW000663

Pomoell,J. and Poedts,S., (2018), EUHFORIA: EUropean Heliospheric FORecasting Information Asset, *J. of Space Weather and Space Climate*, **8**, A35, doi:10.1051/swsc/2018020

Powell,K.G., Roe,P.L., Linde,T.J., Gombosi,T.I. and De Zeeuw,D.L., (1999), A solution adaptive upwind scheme for ideal magnetohydrodynamics, *J. Comput.*

1422   *Phys.*, **154(2)**, 284, doi:10.1006/jcph.1999.6299

1423   Regnier,S. and Fleck,B., (2004), *Proceedings of the SOHO 15 Workshop - Coronal*

1424   *Heating* 6-9 September 2004, St. Andrews, Scotland, UK (ESA SP-575). Ed-

1425   itors: R.W. Walsh, J. Ireland, D. Danesy, B. Fleck. Paris: European Space

1426   Agency, p.519.

1427   Reiss,M.A., Temmer,M., Veronig,A.M., Nikolic,L., Vennerstrom,S., Schongassner,F.

1428   and Hofmeister,S.J., (2016), Verification of high-speed solar wind stream

1429   forecasts using operational solar wind models, *Space Weather*, **14**, 495,

1430   https://doi.org/10.1002/2016SW001390

1431   Richardson,I. and Cane,H., (2017), http://www.srl.caltech.edu/ACE/ASC/DATA/level3/icmetable2.htm.

1432   SHINE Workshops webpage, http://shinecon.org. (2018)

1433   Riley,P. , Linker,J.A. and Mikic,Z.,(2001), Am empirically driven global MHD model

1434   of the solar corona and inner heliosphere, *J. Geophys. Res.*, **106 (A8)**, 15889,

1435   doi:10.1029/2000JA000121

1436   Riley, P., Linker, J.A. and Mikic, Z., (2002). Modeling the heliospheric current sheet:

1437   solar cycle variations, *J. Geophys. Res.*, **107**, 1136, doi:10.1029/2001JA000299

1438   Riley,P., Lionello,R., Linker,J.A., Mikic, Z, Luhmann,J. and Wijaya, J., (2011),

1439   Global MHD Modeling of the Solar Corona and Inner Heliosphere for the

1440   Whole Heliospheric Interval, *Solar Phys.*, **274**, 361, doi:10.1007/s11207-010-

1441   9698-x

1442   Riley,P., Linker,J.A., Lionello,R. and Mikic,Z. (2012), Corotating interac-

1443   tion regions during the recent solar minimum: the power and limita-

1444   tions of global MHD modeling. *J. Atmos. Solar-Terr. Phys.*, **83**, 110. doi:

1445   10.1016/j.jastp.2011.12.013

1446   Riley,P., Ben-Nun,M., Linker,J.A., Mikic,Z., Svalgaard,L., Harvey,J., Bertello,L.,

1447   Hoeksema,T., Liu,Y. and Ulrich,R., (2014), A Multi-Observatory Inter-

1448   Comparison of Line-of-Sight Synoptic Solar Magnetograms *Solar Phys.*, **289**,

1449   769, doi:10.1007/s11207-013-0353-1

1450   Riley,P. Linker,J.A. and Arge,C.N., (2015), On the role played by magnetic ex-

1451   pansion factor in the prediction of solar wind speed, *Space Weather*, **13**, 154,

1452   https://doi.org/10/1002/2014SW001144

1453   Riley,P., Ben-Nun,M., Linker,J.A., Owens,M.J. and Horbury,T.S., (2017), Forecast-

1454   ing the properties of the solar wind using simple pattern recognition, *Space*

1455   *Weather*, **15**, 526, https://doi.org/10.1002/2016SW001589

1456 Roussev,I.I., Gombosi,T.I., Sokolov,I.V., Velli,M., Manchester,W., De Zeeuw,D.L.,

1457   Liewer,P., Toth,G. and Luhmann,J., (2003), A three dimensional model of the

1458   solar wind incorporating solar magnetogram observations, *Astrophys.J.Lett.*,

1459   **595**, L57, doi:10.1086/378878

1460 Rusin,V., Druckmuller,M., Aniol,P., Minarovjech,M., Saniga,M., Mikic,Z., Linker,J.

1461   A., Lionello,R., Riley,P. and Titov, V. S., (2010), Comparing eclipse obser-

1462   vations of the 2008 August 1 solar corona with an MHD model prediction,

1463   *Astron. & Astrophys.*, **513**, A45, doi:10.1051/0004-6361/200912778

1464 Savani,N.P., Collado-Vega,Y., DeForest,C.E., de Koning,C.A., Halford,A., Henley,E.,

1465   Kay,C., Leka,K.D., N. Lugaz,N., MacNeice,P., Mays,M.L., Manchester,W.,

1466   Nieves-Chinchilla,T., Odstrcil,D., Owens,M.J., Patsourakos,S., Poedts,S.,

1467   Rouillard,A.P., Riley,P., Singer,H.J., Shiota,R.D., Steenburgh,R., Verbeke,C.,

1468   Vourlidas,A., Welling,D. and West,M. (2018), Skill metric evaluation by a

1469   Community International Forum for Interplanetary Magnetic Field B_z predic-

1470   tions. *Space Weather*, This Issue.

1471 Schatten,K.H., Wilcox,J.M. and Ness,N.F. (1969), A model of interplanetary and

1472   coronal magnetic fields, *Solar Phys.*, **6**, 442, doi:10.1007/BF00146478

1473 Schatten,K.H., (1971), Current sheet magnetic model for the solar corona, *Cosmic*

1474   *EIectrodynamics*, **2**, 232

1475 Schrijver,C.J. and De Rosa,M.L, (2003), Photospheric and heliospheric magnetic

1476   fields, *Solar Phys.*, **212**, 165, doi:10.1023/A:1022908504100

1477 Schrijver,C.J., De Rosa,M.L., Metcalf,T.R., Liu,Y., McTiernan,J., Regnier,S., Val-

1478   ori,G., Wheatland,M.S. and Wiegelmann,T. (2006) Nonlinear force-free mod-

1479   eling of coronal magnetic fields part I: a quantitative comparison of methods

1480   *Solar Phys.*, **235**,161, doi:10.1007/s11207-006-0068-7

1481 Schrijver,C.J., DeRosa,M.L., Metcalf,T., Barnes,G., Lites,B., Tarbell,T., McTier-

1482   nan,J., Valori,G., Wiegelmann,T., Wheatland,M.S., Amari,T., Aulanier,G.,

1483   Demoulin,P., Fuhrmann,M., Kusano,K., Regnier,S. and Thalmann, J. K,

1484   (2008), Nonlinear Force-free Field Modeling of a Solar Active Region around

1485   the Time of a Major Flare and Coronal Mass Ejection, *Astrophys.J.*, **675**,1637,

1486   doi:10.1088/0004-637X/675/2/1637

Schuck,P.W., (2008), Tracking Vector Magnetograms with the Magnetic Induction Equation, *Astrophys.J.*, **683**, 1134, doi:10.1088/0004-637X/683/2/1134

Schuck,P.W., Antiochos,S.K., Leka,K.D. and Barnes,G., (2016), Achieving Consistent Doppler Measurements From SDO/HMI Vector Field Inversions, *Astrophys.J.*, **823**,101, doi:10.1088/0004-637X/823/2/101

Schuck,P.W., Scherrer,P., Antiochos,S.K. and Hoeksema,T., (2016), Achieving Consistent Vector Magnetic Field Measurements from SDO/HMI, *SDO 2016, Solar Dynamic Observatory, SDO-2016*, SDO Workshop, SDO 2016: Unraveling the Sun's Complexity

Schulz,M., Frazier,E.N. and Boucher,D.J. (1978), Coronal magnetic field model with non-spherical source surface, *Solar Phys.*, **60**, 83, doi:10.1007/BF00152334

Sheeley,N.R. (2017), *Hist. Geo Space Sci.*, **8**, www.hist-geo-space-sci.net/8/21/2017/doi:10.5194/hgss-8-21-2017

Sheeley,N.R. and Wang,Y.-M. (1991), Magnetic field configurations associated with fast solar wind, *Solar Phys.*, **131**, 165, doi:10.1007/BF00151752

Shiota,D., Kataoka,R., Miyoshi,Y., Hara,T., Tao,C., Masunaga,K., Futaana,Y. and Terada,N., (2014), Inner heliosphere MHD modeling system applicable to space weather forecasting for the other planets, *Space Weather*, **12**, 187, https://doi.org/10.1002/2013SW000989

Stevens,M.L., Linker,J.A., Riley,P. and Hughes,W.J., (2012), Underestimates of magnetic flux in coupled MHD model solar wind solutions, *Journal of Atmospheric and Solar-Terrestrial Physics*, **83**, 22, doi:10.1016/j.jastp.2012.02.005

TadesseT., (2015), Effect of the Size of the Computational Domain on Spherical Nonlinear Force-Free Modeling of a Coronal Magnetic Field Using SDO/HMI Data, *Solar Phys.*, **290**, 1159, doi:10.1007/s11207-015-0664-5

TadesseT., Pevtsov,A.A., Wiegelmann,T., MacNeice,P.J. and Gosain,S., (2014) Global solar free magnetic energy and electric current density distribution of Carrington rotation 2124. *Solar Phys.*, **289**, 4031, doi:10.1007/s11207-014-0581-z

Titov,V.S., (2007), Generalized Squashing Factors for Covariant Description of Magnetic Connectivity in the Solar Corona, *Astrophys.J.*, **660**, 863, doi:10.1088/0004-637X/660/2/863

Titov,V.S., Torok,T., Mikic,Z. and Linker,J.A., (2014), A Method for Embedding Circular Force-free Flux Ropes in Potential Magnetic Fields, *Astrophys.J.*, **790**, 163, doi:10.1088/0004-637X/790/2/163

Titov,V.S., Downs,C., Mikic,Z., Torok,T., Linker,J. A. and Caplan,R.M., (2018), Regularized BiotSavart Laws for Modeling Magnetic Flux Ropes, *Astrophys.J.Lett.*, **852**, L21, doi:10.3847/2041-8213/aaa3da

Toth,G., van der Holst,B. and Huang,Z., (2011), Obtaining Potential Field Solutions With Spherical Harmonics and Finite Differences, *Astrophys.J.*, **732**, 102, doi:10.1088/0004-637X/732/2/102

Toth,G., van der Holst,B., Sokolov,I.V., De Zeeuw,D.L., Gombosi,T.I., Fang,F., Manchester,W.B., Meng,X., Najib,D., Powell,K.G., Stout,Q.F., Glocer,A., Ma,Y-J. and Opher,M., (2012), Adaptive numerical algorithms in space weather modeling, *J.Comput.Phys.*, **231**, 870, doi:10.1016/j.jcp.2011.02.006

Toth,G., Sokolov,I.V, Gombosi,T.I., Chesney,D.R., Clauer,C.R., De Zeeuw,D.L, Hansen,K.C., Kane,K.J., Manchester,W.B., Oehmke,R.C., Powell,K.G., Ridley,A.J., Roussev,I.I., Stout,Q.F., Volberg,O., Wolf,R.A., Sazykin,S., Chan ,A., Yu,B. and Kota,J. (2005), Space Weather Modeling Framework: A new tool for the space science community, *J. Geophys. Res.*, **110**, A12226, doi:10.1029/2005JA011126

Upton,L. and Hathaway,D.H. (2014), Effects of Meridional Flow variations on Solar Cycles 23 and 24, *Astrophys.J.*, **792**, 142, doi:10.1088/0004-637X/792/2/142

Usmanov,A.V., (1993), A global numerical 3-D MHD model of the solar wind, *Solar Phys.*, **146**, 377, doi:10.1007/BF00662021

Usmanov,A.V., Goldstein,M.L and Matthaeus,W.H., (2014), Three-Fluid, Three-Dimensional Magnetohydrodynamic Solar Wind Model With Eddy Viscosity and Turbulent Resistivity, *Astrophys. J.*, **788**, 43, doi:10.1088/0004-637X/788/1/43

Usmanov,A.V., Matthaeus,W.H., Goldstein,M.L. and Chhiber,R., (2018), The Steady Global Corona and Solar Wind: A Three-dimensional MHD Simulation with Turbulence Transport and Heating, *Astrophys. J.*, **865**, 25 doi:10.3847/1538-4357/aad6870004-637

van der Holst,B., Sokolov,I.V., Meng,X., Jin,M., Manchester,W.B., Toth,G. and Gombosi,T.I., (2014), Alfven Wave Solar Model (AWSoM): Coronal Heating,

1552   *Astrophys.J.*, **782**, 81, doi:10.1088/0004-637X/782/2/81

1553   Viall,N.M. and Vourlidas,A. (2015), Periodic Density Structures and the Ori-

1554   gin of the Slow Solar Wind, *Astrophys.J.*, **807**, 176, doi:10.1088/0004-

1555   637X/807/2/176

1556   Velli,M. (1993), On the propagation of ideal, linear Alfven waves in radially strati-

1557   fied stellar atmospheres and winds, *Astronomy and Astrophysics*, **270**, 304.

1558   Verdini,A., Velli M., Matthaeus W. H., Oughton S. and Dmitruk P. (2010), A Tur-

1559   bulence Driven Model for Heating and Acceleration of the Fast Wind in Coro-

1560   nal Holes, *Astrophys.J.Lett.*, **708**, L116, doi:10.1088/2041-8205/708/2/L116

1561   Wang,Y.M. and Sheeley,N.R.,Jr. (1990), *Astrophys. J.*, **355**, 726, doi:10.1088/0004-

1562   637X/355/2/726

1563   Warren,H.P., Crump,N.A., Ugarte-Urra,I., Sun,X., Aschwanden,M.J. and Wiegel-

1564   mann,T., Toward a Quantitative Comparison of Magnetic Field Extrapolations

1565   and Observed Coronal Loops *Astrophys.J.*, **860**, 13, 10.3847/1538-4357/aac20b

1566   Welsch,B.T., Abbett,W.P., DeRosa,M.L., Fisher,G.H., Georgoulis,M.K., Kusano,K.,

1567   Longcope,D.W., Ravindra,B. and Schuck,P.W., (2007), Tests and Comparisons

1568   of Velocity-Inversion Techniques, *Astrophys.J.*, **670**, 1434, doi:10.1088/0004-

1569   637X/670/2/1434

1570   Wiegelmann,T., Lagg,A., Solanki,S.K., Inhester,B. and Woch,J. (2005), Comparing

1571   magnetic field extrapolations with measurements of magnetic loops, *Astron.

1572   Astrophys.*, **433**, 701, doi:10.1051/0004-6361:20042421

1573   Wiegelmann,T., (2007), Computing Nonlinear Force-Free Coronal Magnetic Fields in

1574   Spherical Geometry, *Solar Phys.*, **240**, 227, doi:10.1007/s11207-006-0266-3

1575   Wiegelmann,T., (2008) Nonlinear force-free modeling of the solar coronal magnetic

1576   field, *J. Geophys. Res. Space Phys.*, **113**, A03S02, doi:10.1029/2007JA012432

1577   Wiegelmann,T. and Sakurai,T., (2012), Solar force-free magnetic fields, *Living Rev.

1578   Sol. Phys.*, **9**, 5 (2012), doi:10.12942/lrsp-2012-5

1579   Wiegelmann,T., Petrie,G.J.D. and Riley,P., (2017), Coronal Magnetic Field Models,

1580   *Space Sci. Rev.*, **210**, 249, doi:10.1007/s11214-015-0178-3

1581   Wiengarten,T., Kleimann,J., Fichtner,H., Cameron,R., Jiang,J., Kissmann,R. and

1582   Scherer,K., (2013) MHD simulation of the inner heliospheric magnetic field,

1583   *JGR*, **118**, 29, https://doi.org/10.1029/2012JA018089

1584   Wiengarten,T., Oughton,S., Engelbrecht,N.E., Fichtner,H., Kleimann,J. and

1585   Scherer,K., (2016), A Generalized Two-Component Model of Solar Wind

1586   Turbulence and Ab Initio Diffusion Mean-Free Paths and Drift Length-scales

1587   of Cosmic Rays, *Astrophys.J.*, **833**, 17, doi:10.1088/0004-637X/833/2/17

1588   Winebarger,A.R., Lionello,R., Mok,Y., Linker,J.A., and Mikic,Z., (2014), Verification

1589   of Coronal Loop Diagnostics Using Realistic Three-dimensional Hydrodynamic

1590   Models, *Astrophys.J.*, **795**, 138, doi:10.1088/0004-637X/795/2/138

1591   Worden,J, and Harvey,J., (2000), An Evolving Synoptic Magnetic Flux map and

1592   Implications for the Distribution of Photospheric Magnetic Flux, *Solar Phys.*,

1593   *195*, 247, doi:10.1023/A:1005272502885

1594   Yang,W.H., Sturrock,P.A. and Antiochos,S.K., (1986), Force-free magnetic fields:

1595   The magneto-frictional method, *Astrophys. J.*, **309**, 383, doi:10.1088/0004-

1596   637X/309/2/383

1597   Yardley,S.L., MacKay,D.H. and Green,L.M., (2018), Simulating the Coronal Evo-

1598   lution of AR 11437 Using SDO/HMI Magnetograms, *Astrophys.J.*, **852**, 82,

1599   doi:10.1088/0004-637X/852/2/82

1600   Yeates,A.R., Mackay,D.H. and van Ballegooijen,A.A., (2007), Modeling the Global

1601   Solar Corona: Filament Chirality Observations and Surface Simulations, *Solar*

1602   *Phys.*, **245**, 87, doi:10.1007/s11207-VV

1603   Yeates,A.R., Mackay,D.H. and van Ballegooijen,A.A., (2008), Modeling the Global

1604   Solar Corona II: Coronal Evolution and Filament Chirality Comparison, *Solar*

1605   *Phys.*, **247**, 103, doi:10.1007/s11207-007-9013-7

1606   Yeates,A.R. (2014), Coronal Magnetic Field Evolution from 1996 to 2012: Continu-

1607   ous Non-potential Simulations, *Solar. Phys.*, **289**, 631, doi:10.1007/s11207-013-

1608   0301-0

1609   Yeates,A.R., Amari,T., Contopoulos,I., Feng,X., Mackay,D.H., Mikic,Z., Wiegel-

1610   mann,T., Hutton,J., Lowder,C.A., Morgan,H., Petrie,G., Rachmeler,L.A.,

1611   Upton,L.A., Canou,A., Chopin,P., Downs,C., Druckmuller,M., Linker,J.A.,

1612   Seaton,D.B. and Torok,T. (2018), Global Non-Potential Magnetic Models of

1613   the Solar Corona During the March 2015 Eclipse. *Space Sci. Rev.*,**214**, 99,

1614   doi:10.1007/s11214-018-0534-1

1615   Yu,H.S., Jackson,B.V., Hick,P.P., Buffington,A., Odstrcil,D., Wu,C.-C., Davies,J.A.,

1616   Bisi,M.M. and Tokumaru,M. (2015), 3D Reconstruction of Interplanetary

Scintillation (IPS) Remote-Sensing Data: Global Solar Wind Boundaries for Driving 3D-MHD models, *Solar Phys.*, **290**, 2519, doi:10.1007/s11207-015-0685-0

Zhao,X. and Hoeksema,J.T, (1994), A coronal magnetic field model with horizontal volume and sheet currents *Solar Phys.*, **151**, 91, doi:10.1007/BF00654084

Zhu,X. and Wiegelmann,T., (2018), On the extrapolation of magneto-hydro-static equilibria on the sun, arXiv:1809.02168